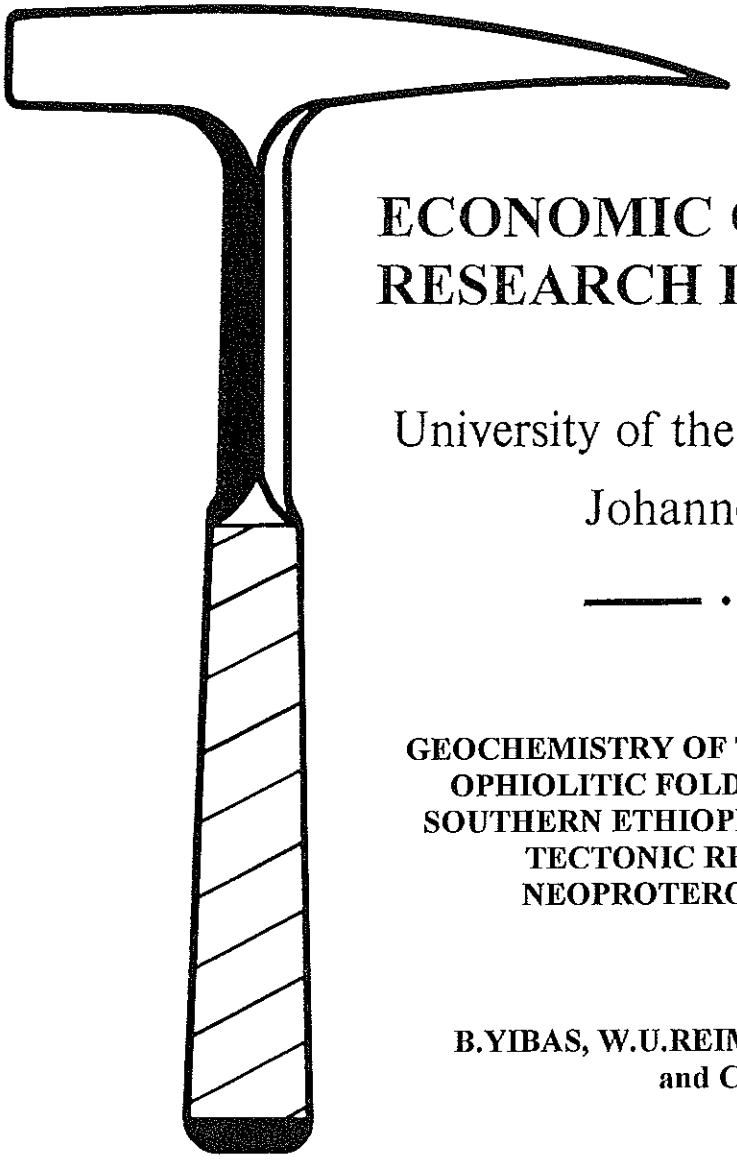

ECONOMIC GEOLOGY RESEARCH INSTITUTE

University of the Witwatersrand

Johannesburg

GEOCHEMISTRY OF THE MAFIC ROCKS OF THE OPHIOLITIC FOLD AND THRUST BELTS OF SOUTHERN ETHIOPIA: CONSTRAINTS ON THE TECTONIC REGIME DURING THE NEOPROTEROZOIC (900 - 700 MA)

B.YIBAS, W.U.REIMOLD, C.R.ANHAEUSSER
and C. KOEBERL

• INFORMATION CIRCULAR No. 349

UNIVERSITY OF THE WITWATERSRAND
JOHANNESBURG

GEOCHEMISTRY OF THE MAFIC ROCKS OF THE OPHIOLITIC FOLD AND THRUST BELTS OF SOUTHERN ETHIOPIA: CONSTRAINTS ON THE TECTONIC REGIME DURING THE NEOPROTEROZOIC (900 - 700 MA)

by

B. YIBAS[1], W. U. REIMOLD[1*], ANHAEUSSER, C.R.[2] AND C. KOEBERL[3]

([1]Geology Department, University of the Witwatersrand, Private Bag 3, Wits 2050, Johannesburg, South Africa

[2] Economic Geology Research Institute, Geology Department, University of the Witwatersrand, Private Bag 3, Wits 2050, Johannesburg, South Africa

[3] Institute of Geochemistry, University of Vienna, Althan Str. 14, A-1090 Vienna, Austria.

** Corresponding Author)*

ECONOMIC GEOLOGY RESEARCH INSTITUTE
INFORMATION CIRCULAR No.349

December, 2000

GEOCHEMISTRY OF THE MAFIC ROCKS OF THE OPHIOLITIC FOLD AND THRUST BELTS OF SOUTHERN ETHIOPIA: CONSTRAINTS ON THE TECTONIC REGIME DURING THE NEOPROTEROZOIC (900 - 700 MA)

ABSTRACT

The mafic rocks of the Neoproterozoic fold and thrust belts in southern Ethiopia are dominantly subalkaline, low-K, low-Ti tholeiitic basalts (LOTI), together with boninites, and minor calc-alkaline basalts. The tholeiitic rocks of the Megado Belt show geochemical characteristics of both N-MORB (normal mid-oceanic-ridge type) and E-MORB (evolved mid-oceanic ridge-type) tholeiites similar to those reported for some Arabian-Nubian Shield gabbros. The Moyale tholeiites are more akin to the N-MORB tholeiites and show higher overall REE abundance than the Megado tholeiites, suggesting a more evolved nature of the Megado tholeiites.

Boninitic lavas occur intercalated with tholeiitic basalts of the Megado and Moyale-El Kur belts. These boninites are dominantly high-Ca boninites, which are genetically associated with MORB rocks. The association of boninites with tholeiites in the Megado and Moyale-El Kur belts suggests that these belts represent ophiolites formed in oceanic supra-subduction zone (SSZ) settings. In contrast, boninites and MORB-type basalts are absent in the Bulbul and Kenticha belts, which are dominated by high-Ti, island-arc tholeiitic and intraoceanic calc-alkaline basalts, which indicate formation in a mature island-arc setting. However, the minor calc-alkaline mafic rocks found in the southern Megado Belt (Geleba area), in the Bulbul Belt and in the Jimma-El Kur sub-belt show geochemical characteristics similar to those of the high-K, calc-alkaline supra-subduction zone (SSZ) basalts from the New Hebrides.

The tectonic setting of the SSZ ophiolites was constrained from differences in the proportions of MORB-type basalts, island-arc tholeiites, and boninites, and the variable compositions of boninites in the Megado and Moyale-El Kur ophiolitic belts. This further allowed the classification of the mafic rocks of these belts into the geochemically distinct Megado, Moyale-1 and Moyale-2 suites. The Geleba and Jimma mafic rocks show transitional geochemical characteristics between the Moyale and Megado suites. The Megado and Moyale-1 suites show stronger subduction characteristics than the Moyale-2 Suite. The Megado Suite is more akin to fore-arc basin and island-arc tholeiites (FAB-IAT). The Moyale-1 suite shows geochemistry transitional between the IAT and MORB-BAB (back-arc basin) mafic suites, whereas the minor Moyale-2 suite shows MORB-BAB affinity with no IAT signature.

The Megado ophiolitic assemblage was formed in a back-arc-type basin but in a fore-arc setting where the generation of boninites and low-Ti tholeiites occurred and was accompanied by sedimentation. In Moyale, the development of the back-arc-type basin was not fully developed, as tensional stresses, needed to achieve splitting of the fore-arc sliver from the mantle wedge, were inadequate. The formation ages of the Moyale, Megado and Bulbul ophiolites in southern Ethiopia are approximately 700, 789+36 and >876+5 Ma, respectively.

oOo

GEOCHEMISTRY OF THE MAFIC ROCKS OF THE OPHIOLITIC FOLD AND THRUST BELTS OF SOUTHERN ETHIOPIA: CONSTRAINTS ON THE TECTONIC REGIME DURING THE NEOPROTEROZOIC (900 - 700 MA)

CONTENTS

oOo

Published by the Economic Geology Research Institute
Department of Geology
University of the Witwatersrand
1 Jan Smuts Avenue
Johannesburg 2001-01-03
www.wits.ac.za/egru

ISBN 1-86838-295-8

GEOCHEMISTRY OF THE MAFIC ROCKS OF THE OPHIOLITIC FOLD AND THRUST BELTS OF SOUTHERN ETHIOPIA: CONSTRAINTS ON THE TECTONIC REGIME DURING THE NEOPROTEROZOIC (900 - 700 MA)

GEOLOGICAL SETTING

Two distinct lithotectonic assemblages (terranes), which are referred to as (1) the granite-gneiss terrane and (2) the mafic-ultramafic-sedimentary ophiolitic assemblages, are recognised in the Precambrian of southern Ethiopia. These assemblages are separated by repeatedly reactivated shear and/or thrust zones (Fig.1; see also Yibas, 2000; Yibas et al., 2000a).
The granite-gneiss terrane has been subdivided into the Burji-Moyale and Adola-Genale sub-terranes, both of which are further subdivided into complexes based on the spatial association of rocks, internal structures, interrelationships of the various rock types, and lithostructural similarity (Yibas et al., 2000a).

The mafic-ultramafic-sedimentary assemblages can be referred to as fold and thrust belts in view of their deformational styles, and as ophiolites, in as far as their origin and lithological association are concerned (Yibas, 2000 and references therein). Four such belts are recognised in the Precambrian of southern Ethiopia. These are the (1) Megado, (2) Kenticha, (3) Bulbul, and (4) Moyale-El Kur belts (Fig. 1).

DESCRIPTIONS OF THE MAFIC ROCKS

The mafic rocks in these belts comprise amphibole-schist, amphibole-chlorite schist, amphibolites and metagabbros. Amphibole schists and amphibolites are the dominant lithologies.

Megado Metabasic Rocks

The Megado Belt occurs in the western part of the Adola area as a linear belt sandwiched between two granite-gneiss blocks of the Adola granite-gneiss complex (Fig. 1). Amphibole schists and amphibolites, together with meta-gabbros, meta-ultramafics, psammitic-pelitic schists, subordinate graphite-schist, graphitic quartzites, and conglomerates, are the dominant lithologic units of the Megado Belt.

The metabasic rocks of the Megado Belt occur as three major linear bodies, separated from each other by mainly metasediments. However, although these linear bodies are separated in space, no significant difference is observed with respect to their mineralogy, texture and mode of occurrence. These bodies comprise amphibole-schists, amphibole-chlorite schist, amphibolites and metagabbros. Amphibole schists and amphibolites are dominant. The meta-gabbros mostly occupy the central parts of the bodies and, in places, are gradational into amphibolites (Yibas, 2000; Yibas et al., 2000a and references therein).

Amphibole-chlorite schists and amphibolites

Amphibole-chlorite schists are fine- to medium-grained and range from amphibole-dominated schists to amphibole-chlorite schists. In the southern part, to the southeast of Digati village, deformed pillow structures are exposed. Representative mineral compositions of the basic schists include (1) actinolite/hornblende (rarely tremolite), albite-oligoclase, epidote-

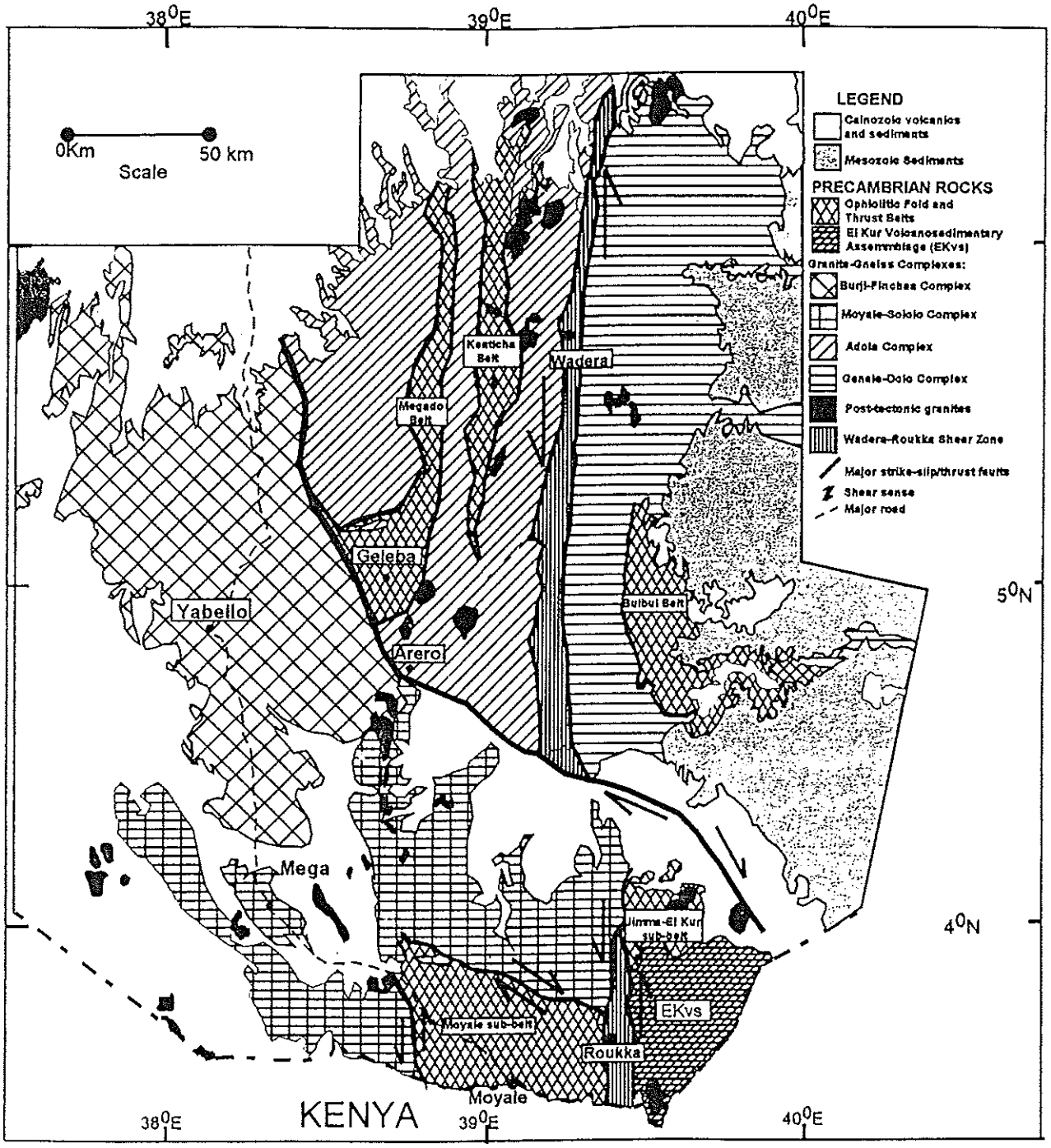

Figure 1: Simplified geological map of the Precambrian of southern Ethiopia (modified after Yibas, 2000).

clinozoisite, chlorite, quartz; (2) actinolite-tremolite/actinolite-hornblende, albite-oligoclase, epidote-clinozoisite, Fe-chlorite, rarely Mg-chlorite, +/- quartz and opaque minerals, and (3) actinolite/hornblende, albite-oligoclase, epidote-clinozoisite, quartz and chlorite.

Subvolcanic amphibolites and gabbro-amphibolites

Lensoidal outcrops of metagabbroic rocks of higher topographic relief and as "cores" within the dominant amphibole-schists and amphibolitic bodies are common. They are medium- to coarse-grained and massive, and, in places, contain pseudomorphs after plagioclase and

pyroxene, now replaced by metamorphic minerals. These rocks are commonly exposed in the central part of the belt and, in places, preserve their intrusive texture, both in outcrop and at the microscopic scale where they typically show granular texture. Hornblende, actinolite, albite, epidote, chlorite, almandine garnet and quartz, in various proportions, are the main minerals found in the meta-gabbroic rocks.

Kenticha Metabasic Rocks

The Kenticha Belt (Fig. 1) mainly comprises ultramafic rocks (serpentinite, talc-tremolite and talc-anthophyllite schists), metabasic rocks, staurolite- and sillimanite-bearing biotite-schists, and minor occurrences of Fe-Mn quartzites, marbles and siliceous metapelites. The Kenticha metabasic rocks are amphibolites, epidote-amphibole gneisses, and amphibole schists. Most commonly, they occur sandwiched between ultramafic bodies as discontinuous bands interlayered with metasediments such as ferruginous quartzites and biotite schists. The meta-basic rocks are composed of actinolite-hornblende, plagioclase, epidote, and quartz, with subordinate amounts of apatite and opaques (most commonly sulphides).

Bulbul Metabasic Rocks

The Bulbul Belt occurs in the easternmost part of the Precambrian of southern Ethiopia (Fig. 1). The belt can be traced across its general N-S strike to the east, following the Dawa River, which exposes the eastern contact of the belt with the biotite and amphibole gneisses of the Negele Formation. The main rock types, which constitute the Bulbul Belt, are amphibolites, chlorite schists, metagabbros, and ultramafic rocks. Slices of quartzofeldspathic gneisses and dioritic mylonites are tectonically interlayered with the basic rocks in the west (Yibas, 2000; Yibas et al., 2000a).

The Bulbul metabasic rocks comprise amphibolites, chlorite-actinolite and chlorite-epidote schists. Metagabbros, tectonically interlayered with mylonitic diorites and granite-gneisses, form the bulk of the Bulbul Belt in the west, whereas extensive outcrops of amphibolites and basic schists occur in the east.

Moyale-El Kur Metabasic Rocks

The Moyale-El Kur Belt covers the area around Moyale town and close to the border of Ethiopia and Kenya and continues into Kenya. It is subdivided into the Moyale and the Jimma-El Kur sub-belts, which are separated by the Roukka shear zone (Fig.1; Yibas et al., 2000a). The main lithologic types in the Moyale sub-belt are metabasic rocks, meta-ultramafics, and minor metasediments (Walsh, 1972; Shagi et al., 1991; Yibas, 2000). The metabasic rocks are mainly amphibolites with local occurrences of amphibole gneisses, amphibole-chlorite schists, and metagabbros. Minor metasediments, such as graphitic schist and quartz-feldspar schists and gneisses, are mainly exposed to the west of Moyale town. The metasediments are invariably intercalated with the basic rocks and ultramafic schists. In some parts of the sub-belt, especially in the western part, mafic rocks can be found intercalated with ultramafic schists, and minor metasediments. The belt was later intruded by the Moyale granodiorite (Yibas, 2000; Yibas et al., 2000a, b).

The eastern part of the Jimma-El Kur sub-belt is covered by Mesozoic sediments. Exposures of the rocks characterising this sub-belt are very scarce. In the central part around El-Kur village, variable rock types occur, including gneissose conglomerates micaceous

quartzofeldspathic schists/gneisses, calc-silicate rocks, ultramafic-mafic schists, serpentinites, marbles and quartzites. Hybrid granitoids, characterised by irregularly mixed gabbroic, dioritic and granodioritic intrusives, form conspicuous hills in the northern part of the sub-belt.

In the central and southern parts of the sub-belt, rare outcrops of gneissose meta-conglomerates, which grade into muscovite-biotite-microcline-quartz schist, ultramafic schists, graphitic schist, and calc-silicates were mapped as the El Kur volcanosedimentary-ultramafic assemblage (Fig. 1; Yibas et al., 2000a).

Moyale amphibolites and amphibole-chlorite schists

The Moyale basic rocks show variable texture and fabric from amphibolite/amphibole gneiss to fine-grained basic schists with lenticular bodies of metagabbro. The amphibolite/amphibole gneiss is a grey, medium-grained rock, which is well foliated and in places banded.

Amphibolite and amphibole gneiss represent the largest proportion of the rocks in the Moyale sub-belt. In the western part, these rocks are in tectonic contact with the Moyale gneissic rocks, whereas in the east, they grade into amphibolites and basic schists, often with garnet porphyroblasts.

Low relief outcrops of amphibolites are most abundant in the eastern part of the Moyale sub-belt, where they occur intercalated with ultramafic rocks. Altered amphibolites and basic schists, interlayered with altered ultramafics, are dominant in the eastern part. Elongated pillow-like blocks found within the altered basic schists suggest the possible submarine extrusion of these rocks.

Towards the east, the metagabbros become coarser-grained and less foliated. Massive sulphide-bearing blocks of amphibolite occur overlying foliated amphibole schists. Further to the southeast, a light grey, well-foliated and sheared, coarse-grained amphibole gneiss underlies the non-foliated amphibolite. Amphibole gneisses occur intercalated with amphibole schists and less foliated granular gabbro-dioritic rocks, suggesting primary magmatic layering involving fine-grained basic rocks (volcanic), gabbros, ultramafics, and dioritic rocks. The succession shows layering from coarse-grained gabbroic rock to well-foliated, fine- to medium-grained amphibolites. Migmatitic amphibole gneisses occur close to the Moyale Granodiorite. Metagabbroic rocks occur intermittently as circular to elliptical bodies intrusive into the amphibolites of eastern Moyale.

Moyale garnet-bearing amphibolite and amphibole-chlorite schists

These rocks occur in the easternmost part of the Moyale sub-belt, southwest of Roukka village. Garnet-bearing amphibolites and amphibole-chlorite schists occur close to the Ethiopian-Kenyan border.. The garnet-bearing varieties are grey, medium-grained, well foliated, and, in places, finely banded into thin leucocratic and melanocratic layers. Hornblende-actinolite, garnet (porphyroblasts up to 10 mm in diameter), plagioclase, quartz, and chlorite are the major minerals in the amphibolites and amphibole-chlorite schists.

Jimma-El Kur Metabasic Rocks

Amphibolites and amphibole schists intercalated with various proportions of metasediments and subordinate ultramafic rocks occur in the northern part of the complex, around 04^0 N latitude. Extensive outcrops of amphibolite and gabbro-amphibolite form a ridge near the

water-well at Jimma village. Minor amounts of quartzites and ultramafic rocks occur interlayered with the metabasic rocks.

The metamorphic signature of the mafic suites in the Precambrian of southern Ethiopia, as seen in the mineral assemblages of these rocks, indicates metamorphic grade not exceeding the greenschist-amphibolite transition facies of Turner (1981). Locally, however, mid-amphibolite facies metamorphism is evident where garnet porphyroblasts are developed.

GEOCHEMISTRY

Sample Preparation and Chemical Analyses

Sample preparation was carried out at the Geology Department, University of the Witwatersrand, Johannesburg, South Africa and in the Central Laboratory of the Ethiopian Institute of the Geological Surveys, Addis Ababa, Ethiopia. Samples used for geochemical analysis were milled using chrome-steel discs in a rotary mill. Major and trace elements were analysed by XRF on fused glass discs and powder pellets in the Geology Department at the University of the Witwatersrand, Johannesburg. Trace element concentrations were determined by instrumental neutron activation analysis (INAA) at the Institute of Geochemistry, University of Vienna, using methods described by Koeberl et al. (1987) and Koeberl (1993). Additional trace elements, including REE, were determined using ICP-MS at the Anglo American Research Laboratory, Johannesburg (compare Yibas, 2000 for detail). All the major and trace element analyses and normative compositions discussed in this paper are listed in the Appendix Table 1.

General Geochemical Characteristics

Determining the original chemistry of a metamorphosed rock is rendered possible with the combined use of both major and trace elements. The low-grade mafic suites of southern Ethiopia show no significant alteration, although silica veins are common and clearly defined alteration zones may be associated with shearing. Alteration zones of this type are often associated with gold mineralisation (e.g., in the Moyale area, and in the Mi-essa Ridge south of Digati village in the Megado Belt). Significant carbonatization, saussuritization, silicification and oxidation also took place in these zones (e.g., in the Mi-essa Ridge in the Megado Belt). Samples of the various basic rocks were collected away from such alteration zones whenever possible. The geochemical data (Appendix Table 1) were then screened to determine whether alteration due to metamorphism and/or weathering may have affected the original chemistry of the rocks.

Plotting of the alkali elements into a ($K_2O + Na_2O$) vs ($K_2O/(K_2O + Na_2O)$ X 100 diagram (Fig. 2) together with the concentration ranges of the major element oxides (Table 1), indicates that chemical heterogeneity due to alteration is minimal for most of the sample groups. However, some samples from the Bulbul Belt plot into the spilitic field and other samples from the Moyale Belt and the El-Kur sub-belt plot outside the igneous field (Fig. 2), and were discarded.

Variation diagrams of most major elements plotted against SiO_2 show systematic trends (e.g., TiO_2, MgO, MnO, CaO, $Fe_2O_3^T$), which can be explained by differentiation. Likewise, the trace elements V, Cr, Co and Ni show negative correlation, whereas Sr, Rb, Zr, Nb and the

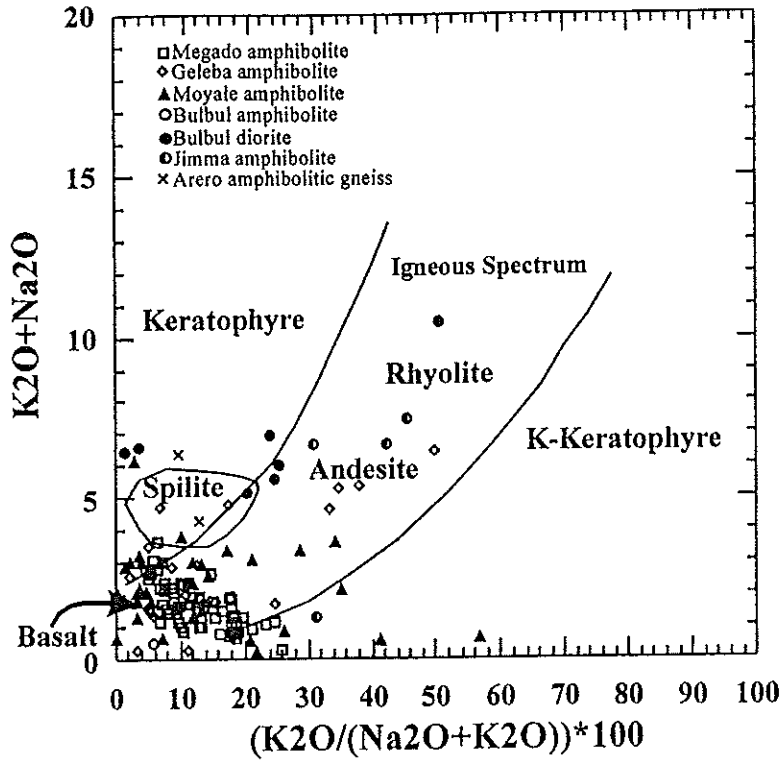

Figure 2: Plot of the Precambrian metabasic rocks of southern Ethiopia showing the effect of alteration on primary chemical compositions (after Hughes, 1973).

REE show positive correlation with SiO_2. However, most of the mobile elements such as Rb and Sr show a wider scatter than the HFS (high field strength) elements, such as Zr, Nb and Y.

Plots of major elements against MgO are most suitable for mafic rocks, for which the range in SiO_2 concentration may be small. MgO is an important component of the solid phases in equilibrium with mafic melts and shows a great deal of variation either as a consequence of the breakdown of magnesian phases during partial melting or their removal during fractional crystallisation (Rollinson, 1993). Plots of the oxides and the trace elements versus MgO (Fig. 3) are intended to reveal how much of the original chemistry is affected by alteration and metamorphism. On the variation diagrams of major elements against MgO (Fig. 3a), TiO_2, K_2O, and P_2O_5 show strong negative correlation with MgO, whereas CaO, total FeO, and MnO show positive correlation. SiO_2, Na_2O, K_2O and Al_2O_3 show slight negative correlation with MgO for most of the samples of each basaltic suite.

Zr is considered one of the most immobile elements and is little affected by metamorphism and alteration (Pearce and Cann, 1973; Cann, 1970). Therefore, the co-variation of an element with Zr could more likely be interpreted in terms of original chemical composition related to igneous processes such as differentiation, rather than to alteration. Among the major element oxides TiO_2 and P_2O_5 and, to a lesser extent, MnO, K_2O and SiO_2 show positive correlation with Zr, whereas MgO and CaO show slight negative correlation (Fig. 4a). This negative MgO and CaO correlation with Zr is consistent with early crystallising minerals such as olivine, pyroxene and Ca-plagioclase forming during magma differentiation. The rest of the oxides show a wide scatter and poorly defined trends, suggesting probable secondary effects.

Among the trace elements, Y, Sr, Nb, Hf, Zn, Rb and Ba show positive correlation, and Cr, Ni, Co and V negative correlation with Zr (Fig. 4b).

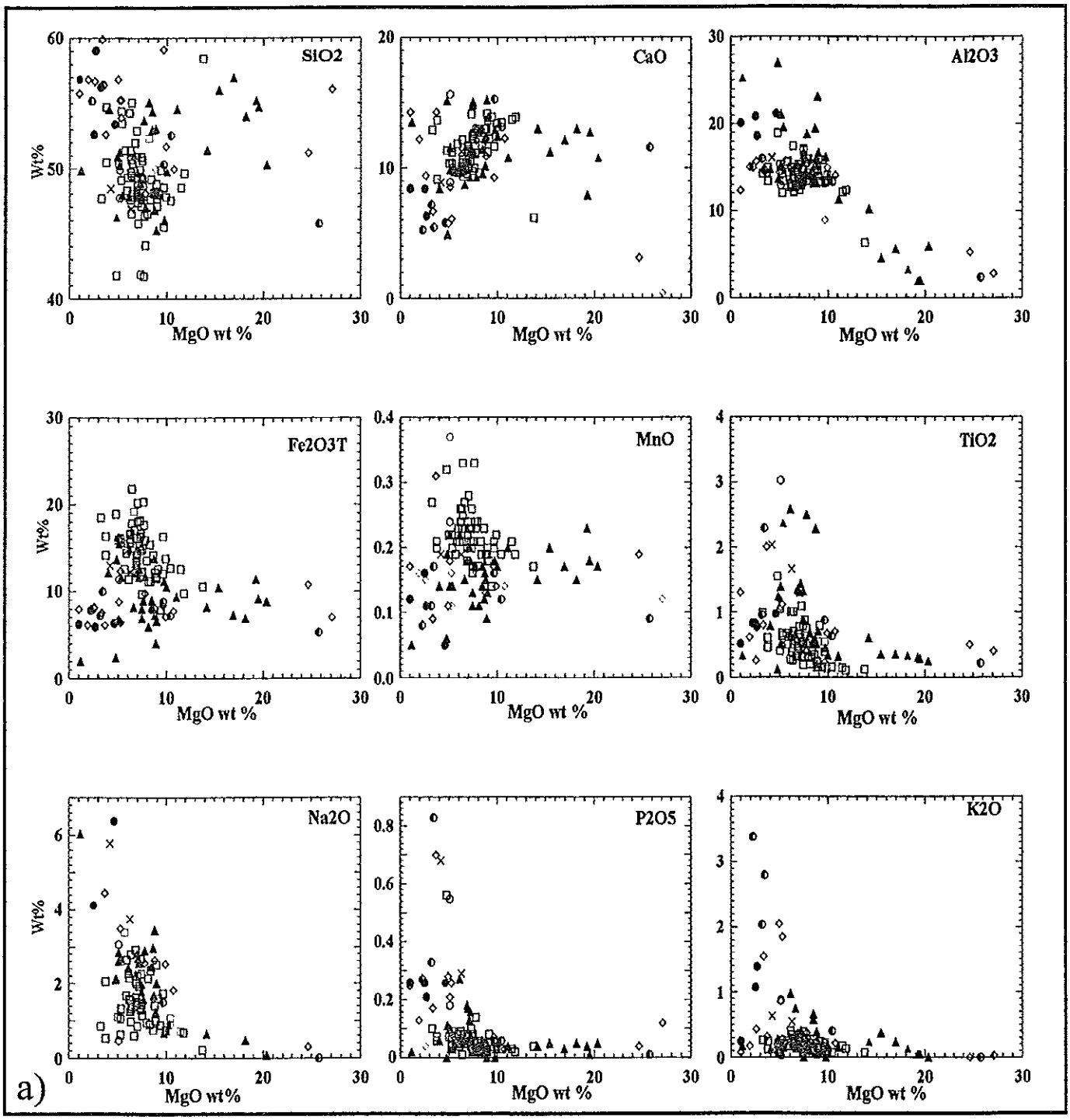

Figure 3 : MgO vs major and trace elements of the Precambrian basic rocks of southern Ethiopia; $Fe_2O_3^T$ = total Fe as Fe_2O_3; trace element data in ppm. Symbols as in previous diagrams.

Figure 3 (contd).

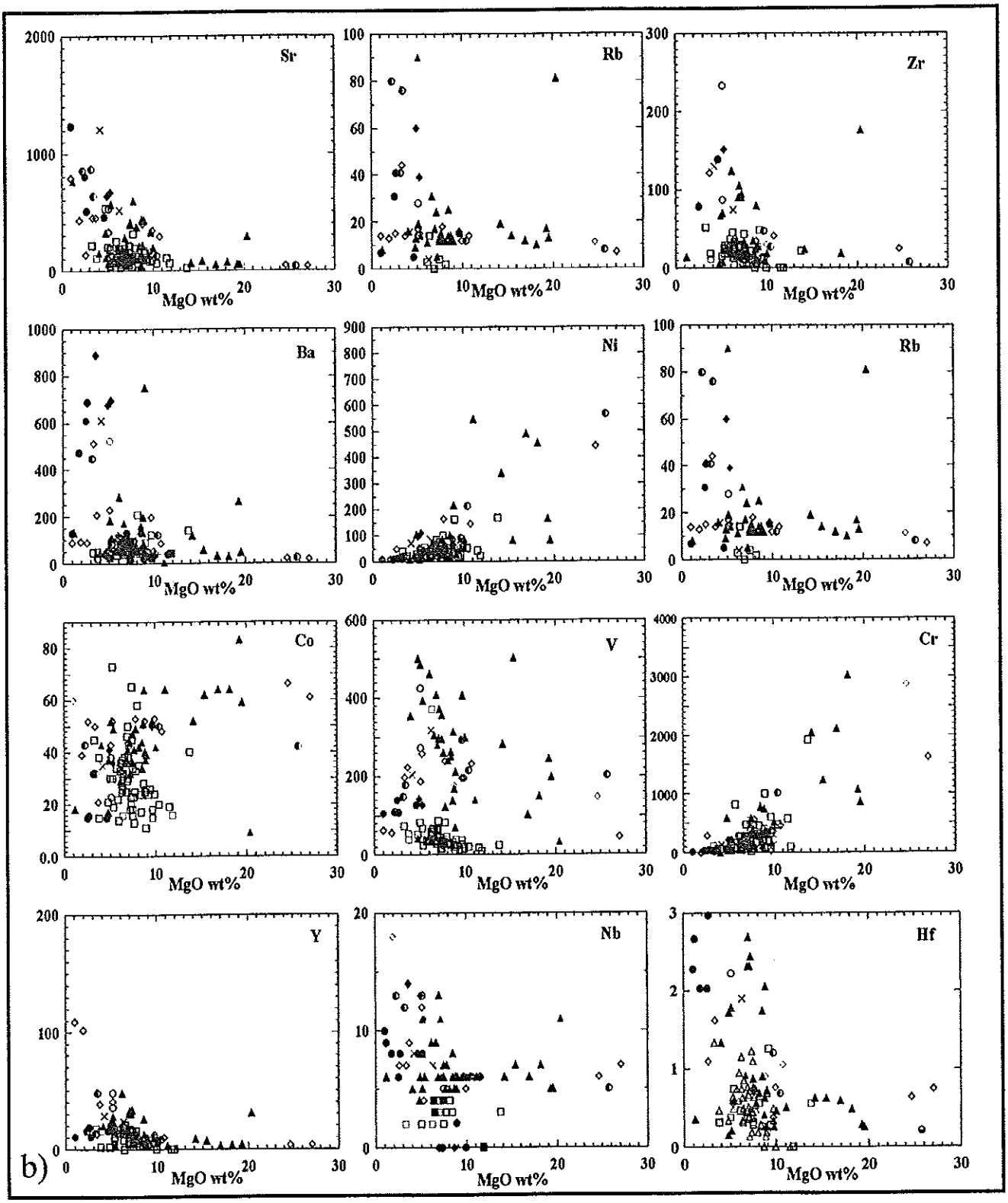

The chemical characteristics observed in the basaltic suites of southern Ethiopia can be summarised as an increase in Ti, Zr, P, Y, V, Zn and REE with decreasing MgO, Ni, Cr, V, and Sr (Figs. 3 and 4). Fractional crystallisation of mineral phases such as clinopyroxene, plagioclase, olivine, and possibly orthopyroxene could explain these chemical characteristics.

TiO_2, P_2O_5, MgO, Y, V and REEs show systematic variations with Zr (Fig. 4), suggesting the limited mobility of these elements during metamorphism and alteration. Ti, Zr, Nb, Y and REEs are among the elements considered to be relatively immobile and, thus, are commonly used to investigate the types of protolithic magma, degree of differentiation, and possible tectonic setting (e.g. Pearce and Norry, 1979; Winchester and Floyd, 1977). Based on these findings, it is possible to use these elements to establish parental geochemical characteristics (type of magma and degree of differentiation) and the tectonic setting of the low-grade volcanosedimentary-ultramafic belts of southern Ethiopia.

Nature of Magma and Rock Classification

The mafic rocks in the Megado Belt can be grouped geochemically into the Megado and the Geleba groups (compare Tables 1a and 1b).

The SiO_2 concentrations in the Megado mafic rocks range from 41.7 to 54.7 wt%, most MgO values fall into the range from 5 to 10 wt%, and TiO_2 concentrations range from 0.11 to 0.8 wt%. Most of the samples have FeO^*/MgO (FeO^* = total Fe) ratios between 0.6 and 3.5; however, a few samples show values as high as 5.08. The Mg# (100 x Mg ($Mg + Fe_T^{+2}$)) of most samples is between 40 and 70 wt%. Al_2O_3 ranges from 12 to 18 wt%, $Fe_2O_3^T$ (total iron as Fe_2O_3) is between 10 and 20 wt%, and MnO between 0.15 and 0.34 wt%.

The Megado mafic suites, in general, show higher iron (10-20 wt%) and MnO ($\geq$ 0.2 wt%) than the other suites (Table 1a).

The Geleba mafic rocks, from the southern part of the Megado Belt, are represented by amphibolites, with subordinate metagabbros and metadiorites and, hence, have a wider SiO_2 range (48-60 wt%) than the Megado and Moyale mafic suites (Table 1a, b). TiO_2 in the Geleba rocks ranges from 0.2 to 2.0 wt%. The TiO_2 vs SiO_2 variation diagram (Fig. 3) shows the presence of two populations in the Geleba suite. Group-1 has TiO_2 values ranging from 0.5 to 2.0 wt%, and SiO_2 from 50 to 60 wt%, whereas Group-2 shows lower TiO_2 (0.2-0.8 wt%) and SiO_2 ranges from 48 to 57 wt%.

Based on their SiO_2 concentrations (47.5 to 56.8 wt%), the basic rocks of the Bulbul Belt can be classified into two groups (Table 1). Group-1 samples have SiO_2 concentrations from 47.5 to 50 wt%, with high TiO_2 (3.03-1.05 wt%), Al_2O_3 (13-14.6 wt%), total Fe (11.5-16 wt%), MnO (0.24-0.4 wt%), MgO (about 5 wt%), and CaO and (9-15.6 wt%), as well as variable Na_2O (3.07 to 0.49 wt%), K_2O (0.03-0.87 wt%) and P_2O_5 (0.18-0.55 wt%). Group-1 rocks also show a wide variation in their TiO_2, P_2O_5, CaO, alkali element and P_2O_5 values, whereas Group-2 shows narrow ranges in their major element chemistry. Group-2 basic rocks also have SiO_2 values from 52.6 to 56.8 wt%, TiO_2 (0.52-1 wt%), high Al_2O_3 (20-21 wt%), total Fe (6-8 wt%), MnO (0.05-0.16 wt%), MgO (1-4.6 wt%), CaO (5.5-8.4 wt%), Na_2O (4-6.4 wt%), K_2O (0.25-1.1 wt%) and P_2O_5 (0.26 wt%).

The major elements of the mafic rocks of the Moyale Belt also define two distinct groups (Table 1). Group-1 contains high MgO (7-12 wt%) rocks with SiO_2 >50 wt% and low TiO_2, with most samples having < 0.4 wt%. Group-2 rocks are dominantly metabasalts with SiO_2 <50 wt% and some andesitic rocks. A few Group-2 samples exhibit high TiO_2 values (>1.5 wt%). The presence of high magnesian andesitic rocks in the Moyale Belt is also apparent on the MgO versus major element diagrams (Fig. 3a).

The rocks of the Jimma-El Kur Sub-belt show SiO_2 concentrations from 45.8 to 56.4 wt%, with most samples having >50 wt%. A few samples exhibit high MgO contents (>8 wt%) and

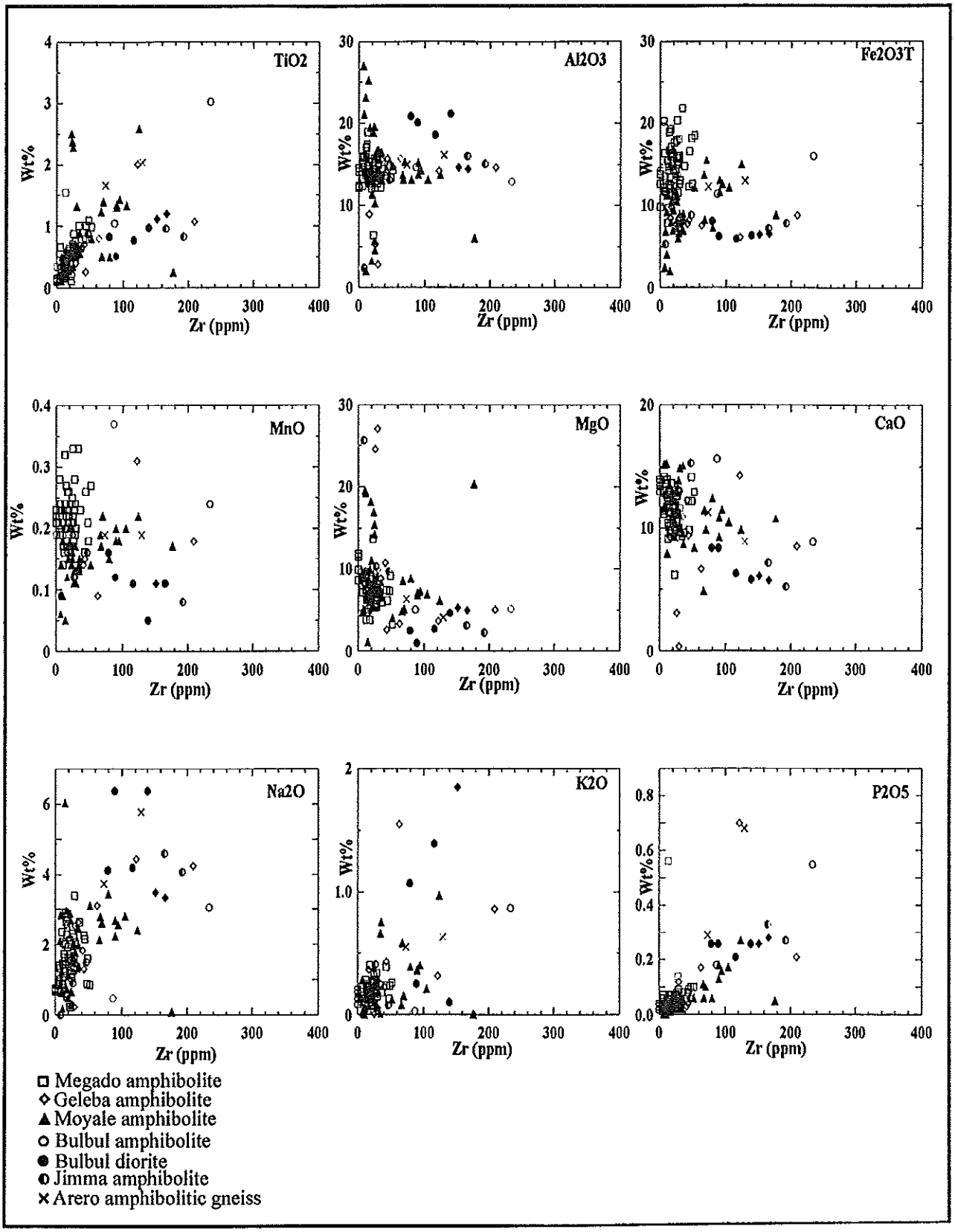

Figure 4: Plots of Zr vs major and trace elements for the Precambrian metabasic rocks of southern Ethiopia.

Figure 4 (Contd).

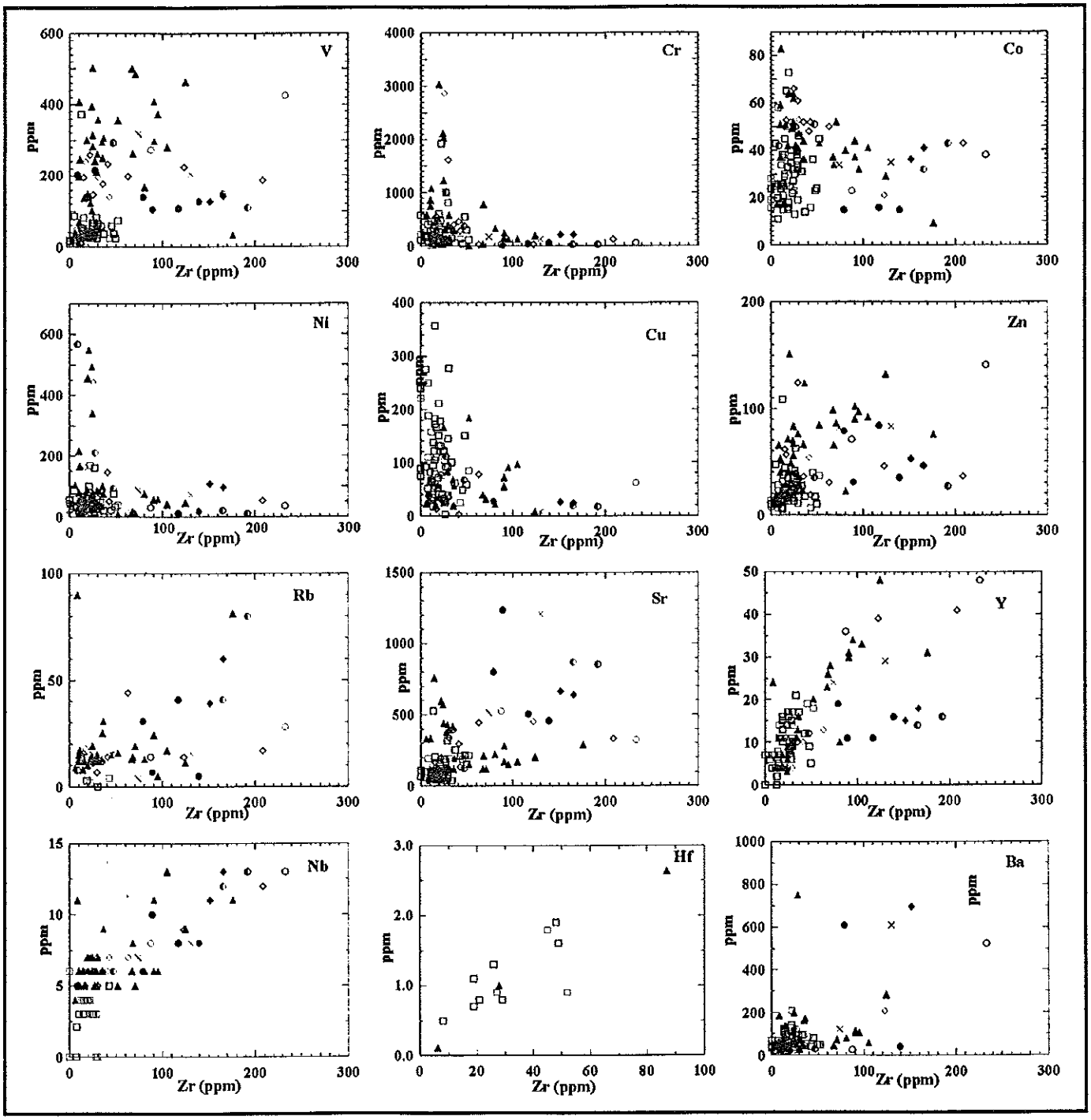

TiO_2 concentrations from 0.1 to 0.6 wt%, with the exception of one sample (JE97132c), which has a TiO_2 content of 2.3 wt%. This sample also has relatively high total Fe and slightly higher MnO and P_2O_5 (Table 1, Fig. 3a).

With the exception of the Bulbul rocks and a few samples from the Jimma-El Kur sub-belt, which straddle the alkaline and sub-alkaline boundaries on the alkaline vs. sub-alkaline discrimination diagrams, most samples exhibit subalkaline affinity (Fig. 5a). The majority of the El-Kur and Bulbul rocks straddle the boundary between the tholeiitic and calc-alkaline fields on the AFM diagram (Fig. 5b). Most Geleba mafic rocks and high-Mg andesites show

calc-alkaline affinities. Clearly, the data for the low-grade mafic rocks from the Precambrian of southern Ethiopia show the dominance of subalkaline, low-K, low-Ti (LOTI), tholeiitic basalts, with minor andesitic basalts and andesites (Fig. 5). The subalkaline rocks are quartz-normative and olivine-hypersthene-normative (CIPW data), whereas the alkaline rocks are nepheline normative (Table 1).

Low P_2O_5, low Zr and an increase of Ti with increasing Zr further corroborate the dominance of tholeiitic basaltic rocks. The Y and Nb values of a few samples, mainly from the Moyale mafic suite, are similar to alkali basalts of both oceanic and continental affinity. However, the Y/Nb ratio could also be lower due to possible crustal contamination of mantle-derived magmas (e.g., Wilson, 1989).

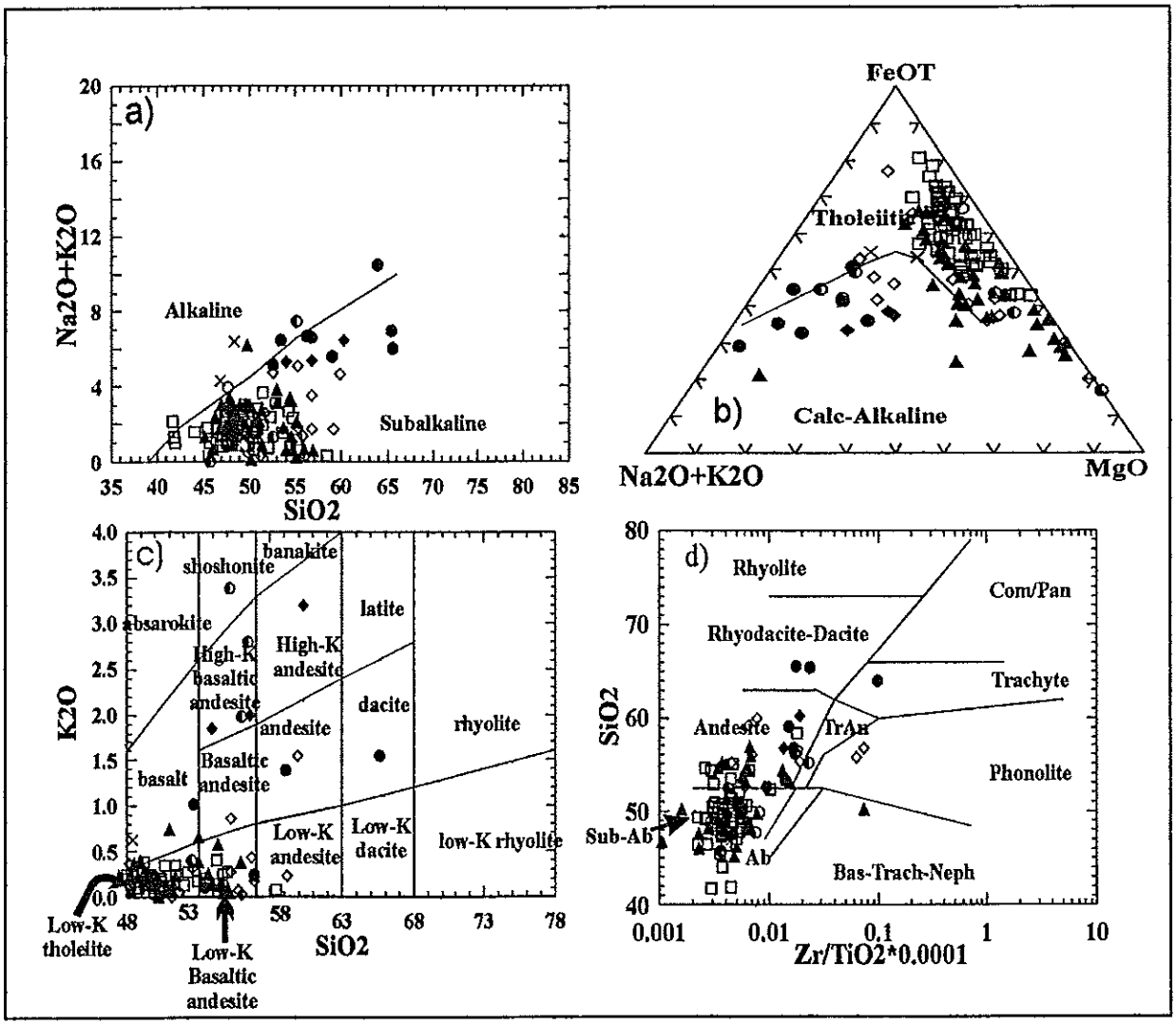

Figure 5: Rock classification of the Precambrian metabasic rocks of southern Ethiopia. Diagrams: after (a) Miyashiro (1975), (b) Irvine and Baragar (1971), (c) De la Roche et al. (1978), and (d) Winchester and Floyd (1977). Symbols as in Figure 4.

Most of the calc-alkaline andesite samples in the study area show boninitic affinity in that they have high SiO_2 (≥50 wt%), high MgO (>7 wt%), and low TiO_2. Yibas (1993), Woldehaimanot and Behrmann (1995) and Wolde et al. (1996) recorded the presence of boninites in the Megado Belt, but these rocks have not been reported from the other belts (cf. below).

REE Geochemistry

The possibility that REE patterns might be affected by sea-floor alteration and low-grade metamorphism has been discussed by, for example, Pearce and Cann (1973), Pearce (1975), Frey (1983), Frey and Green (1974) and Frey et al. (1978). Some tests are, therefore, necessary to understand the effect of alteration and metamorphism on the REE chemistry of the samples under discussion before using the REE geochemical patterns to understand the petrogenesis of the rocks. One of the most reliable tests involves plotting the REE abundances against Zr. Figure 6 illustrates that the REE elements for these sample suites show a systematic increase with increase of Zr concentrations. This suggests that the overall REE patterns have not changed significantly by alteration and metamorphism.

As tholeiitic and boninitic rocks are recognised in the mafic suites of southern Ethiopia, the REE patterns of these two rock suites are treated separately to determine if the REE patterns support these classifications (Fig. 7).

Tholeiitic rocks

Megado tholeiites

The Megado tholeiitic rocks display two distinct REE patterns, both of which show overall REE concentrations that are higher than those of the boninitic series (Figs. 6, 7). Group-1 (Fig. 7a) shows low overall REE fractionation ($(La/Yb)_N$ = 0.98-1.75) and a strong positive Eu anomaly.

The LREEs show systematic enrichment with differentiation (i.e., with increase of the $Fe_2O_3^T/MgO$ ratio) in that there is a transition from depletion ($(La/Sm)_N$ <1) to a flat LREE pattern to enrichment with La/Sm_N>1. The HREE pattern changes from enrichment to flat patterns with differentiation ($(Tb/Yb)_N$ from 2.5 to 0.98).

Moyale tholeiites

The Moyale tholeiitic rocks also show two distinct groups of REE patterns. The amphibolites and amphibole-chlorite schists have relatively higher overall REE abundance with patterns progressively changing from tilting-downward towards HREE to flat patterns, as the REE concentration increases with increasing differentiation (Fig. 7d). These patterns are also characterised by strong positive Eu anomalies, which die out with the increase of the overall REE concentrations, corresponding to differentiation. They also show overall REE enrichments ($(La/Yb)_N$ = 2.54-4.19), strong LREE enrichment for most samples ($(La/Sm)_N$ = 1,37-3.89), and flat to depleted HREE patterns ($(Tb/Yb)_N$ = 0.88-2.00). Sample 97059C from this group shows anomalous concentrations for La (19.5 ppm) and Tm (1.8 ppm), which give rise to an anomalous U-pattern. An aplitic dyke intruded this rock resulting in the REE contents of the sample probably being contaminated by the dyke.

The REE patterns for the garnet-bearing amphibolite and amphibole schists from the eastern part of the Moyale Belt have lower REE abundance than their western counterparts. They are relatively enriched in La, but show variable concentrations of Yb. Otherwise, they show an overall flat REE pattern ($(Ce/Yb)_N$ = 10-1.75), with a slight positive Eu anomaly which is subdued by the associated positive Sm anomaly. Sample M297101A differs from the other samples in this group in that it has lower REE concentrations and differentiated REE patterns (Fig. 7b).

The REE patterns for the Moyale tholeiites are distinctly different from those of the Megado tholeiites. The Moyale tholeiites have higher REE abundances, especially higher Ce

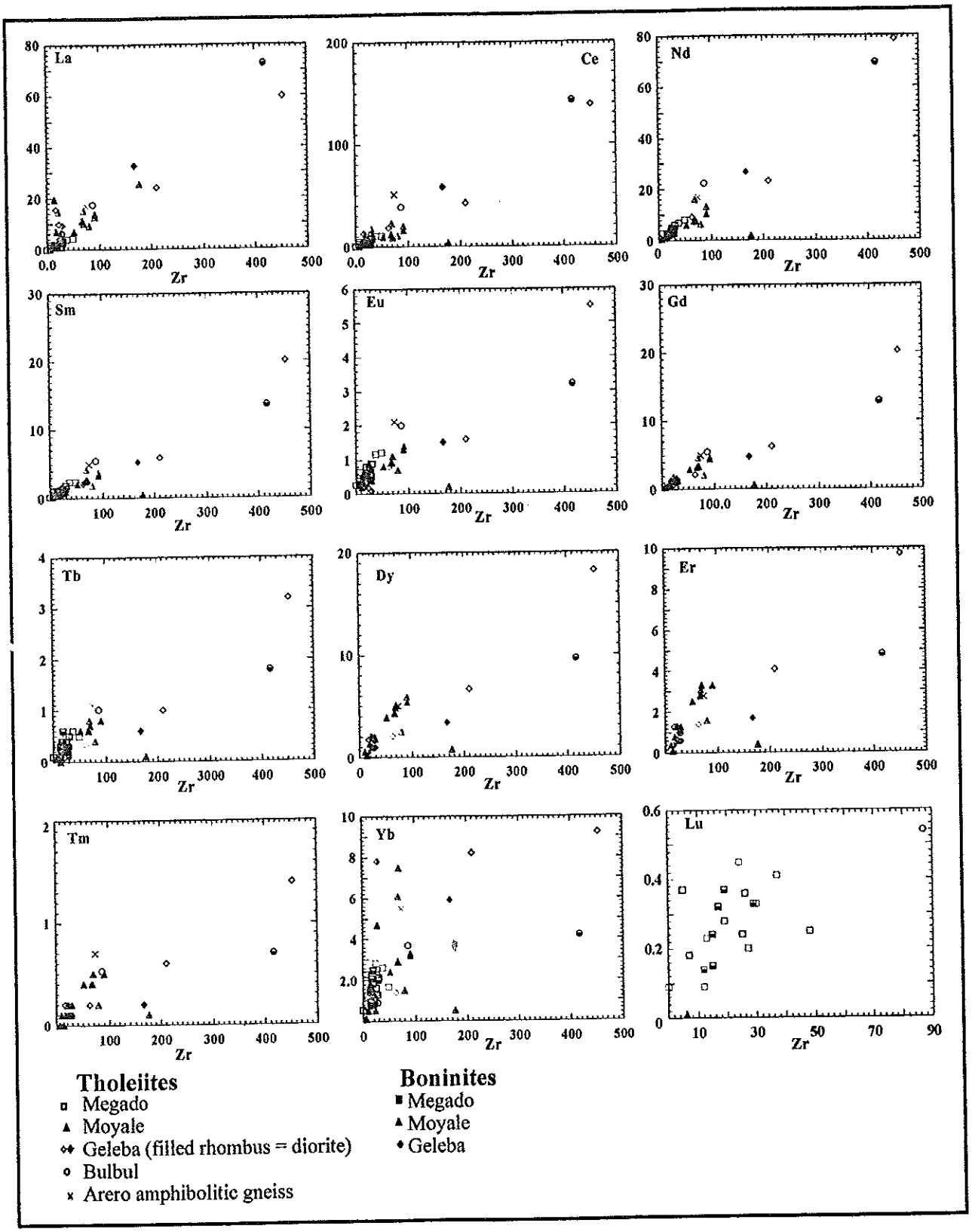

Figure 6 : Plots of Zr vs rare earth elements (data in ppm) of the Precambrian metabasic rocks of southern Ethiopia.

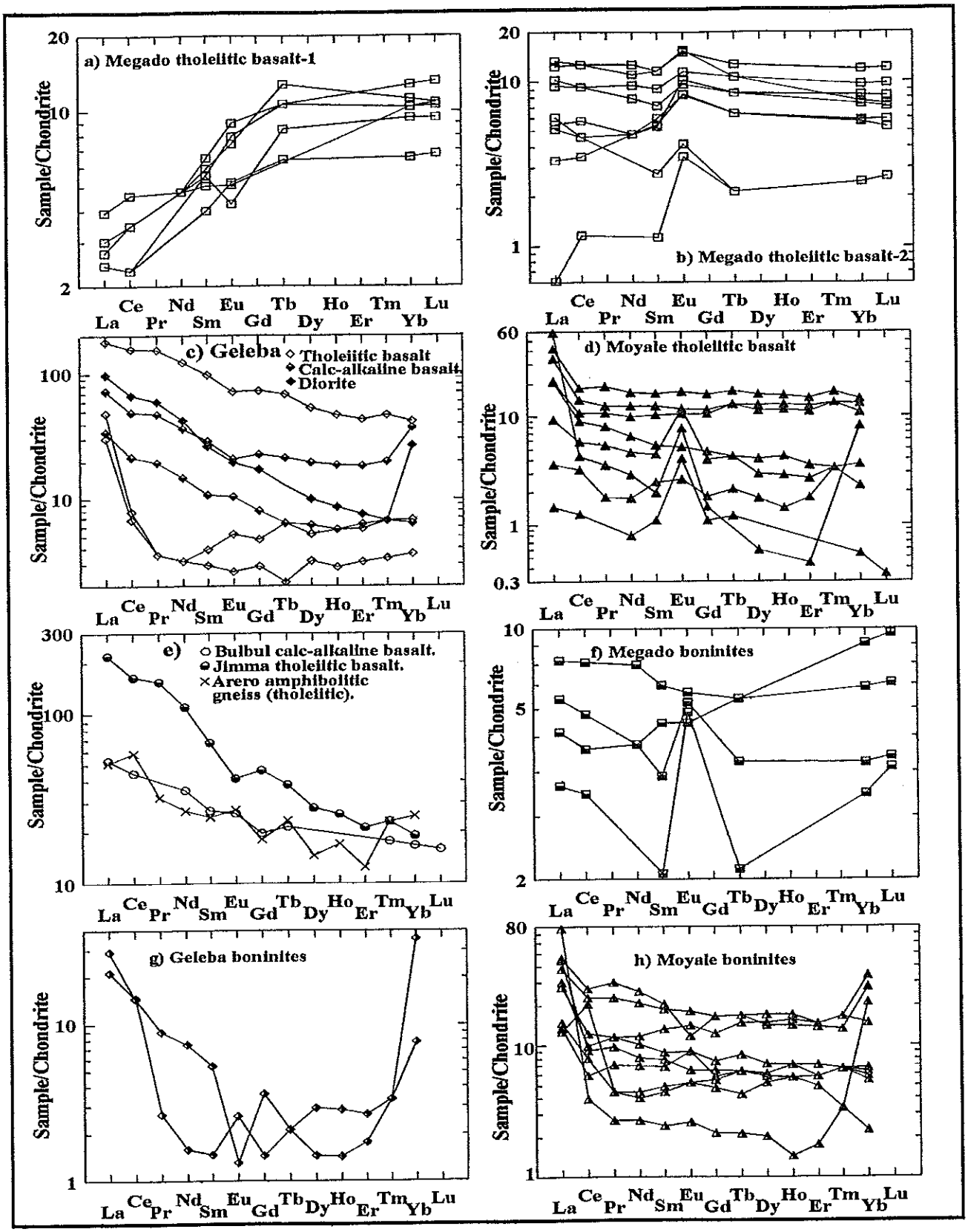

Figure 7: Chondrite-normalised REE patterns for the Precambrian metabasic rocks of southern Ethiopia. Chondrite (C1) normalisation factors from Nakamura (1974). See text for discussion.

concentrations, and their positive Eu anomalies die out with increasing differentiation. The Megado tholeiites also have strongly depleted LREE patterns, unlike the Moyale tholeiites that have moderate LREE enrichment. The Moyale REE patterns are more similar to N-MORB patterns, whereas those of the Megado samples are similar to those of more evolved oceanic tholeiites (E-MORB) and back-arc tholeiites (e.g., Crawford and Keays, 1987).

Calc-alkaline rocks

Minor occurrences of calc-alkaline lavas have been recognised amongst the mafic suites from Bulbul, Geleba (southern Megado) and Jimma-El Kur. The REE patterns of the Bulbul and Jimma-El Kur mafic rocks are strongly LREE-enriched and HREE-depleted. However, in contrast to the Bulbul rocks that show negative Eu anomalies, the Jimma-El Kur samples show no Eu anomalies (Fig. 7e).

The calc-alkaline andesites and diorites of Geleba display higher overall REE abundance, strong LREE enrichment, and HREE depletion. However, a few samples show enrichment in Yb. A REE pattern for a coarse-grained, gneissose amphibolite interlayered with quartzofeldspathic gneisses from south of Arero village (Fig. 1) is characterised by a steep, downward slope towards the HREE. However, the middle REEs show a strongly differentiated pattern with a positive Eu anomaly. This amphibolite gneiss displays similar geochemical characteristics to those of the calc-alkaline rocks of the Bulbul Belt (Fig. 7e).

Boninites

The boninitic rocks in the various mafic suites show an overall similarity in that all display U-shaped REE patterns with or without positive or negative Eu anomalies, although each boninitic suite shows its own distinct pattern (Figs. 7f-h).

The Megado boninites display strong LREE enrichment and strongly to moderately enriched HREE patterns (Fig. 7f). The positive Eu anomaly dies out with increase in the overall REE abundance. The boninites from Geleba display pronounced U-shaped patterns with strongly enriched HREE and LREE patterns and variable Eu anomalies (Fig. 7g). The Moyale boninites show much more pronounced U-shapes, with most samples having positive Eu anomalies. However, negative Eu anomalies are also not uncommon (Fig. 7h).

The REE patterns exhibited by the metaboninites of southern Ethiopia are similar to the REE patterns of the boninites from New Caledonia (Cameron, 1989). However, the southern Ethiopian boninites exhibit positive Eu anomalies. The variation in the Eu character could be explained by variable plagioclase accumulation.

The U-shaped REE patterns of the boninites are not typical features of arc rocks. LREE enrichment in boninites could result from metasomatism of their harzburgitic sources by an LREE- and Zr-enriched fluid (Sun and Nesbitt, 1977; Jenner 1981; Hickey and Frey, 1981; Cameron et al., 1983; Nelson et al., 1984; Hickey-Vargas, 1989).

Spider Diagrams of Selected Elements

Tholeiites

Megado tholeiites

Although they have many features in common, the spider diagrams for the samples from the Megado tholeiites can be subdivided into two groups (Figs. 8a ,b). Group-1 tholeiites lack the

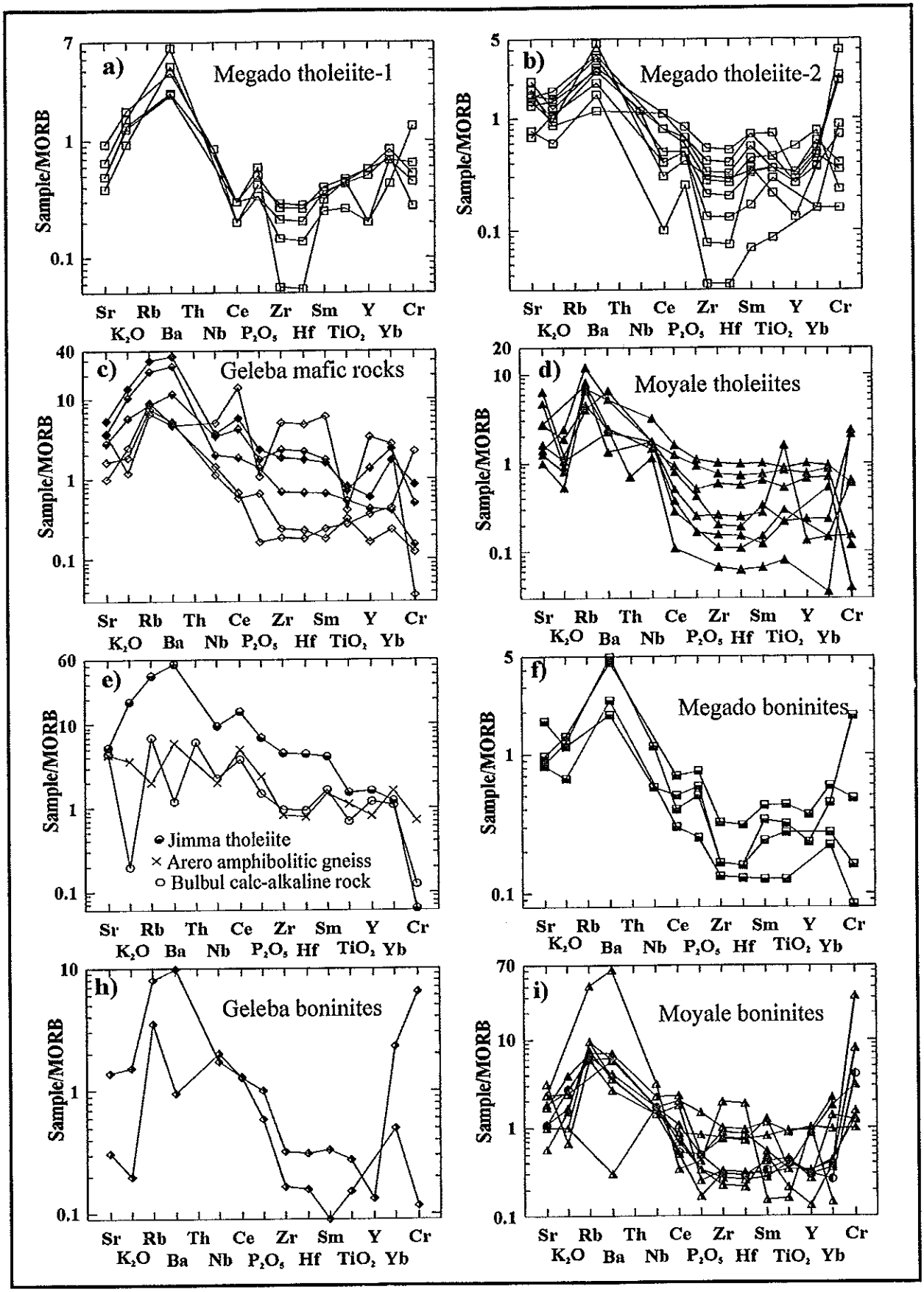

Figure 8: Trace and minor element spider diagram plots for the Precambrian metabasic rocks of southern Ethiopia (normalisation data from Pearce, 1983).

troughs at K_2O and Y when compared with Group-2 tholeiites, which also show higher Cr concentrations than the Group-1 tholeiites (cf. Figs. 8a, b).

In general, the Megado tholeiites show spider diagrams resembling those of E-MORB (evolved-MORB) (Pearce et al., 1984). The Megado rocks also show relatively stronger differentiation and lower overall abundance, especially with respect to their HFS elements. E-type MORB (also known as P-type MORB) are ocean-floor basalts from plume-influenced regions such as Iceland, which are generally enriched in incompatible trace elements (Rollinson, 1993).

The Geleba tholeiites from the southern part of the Megado Belt also show two contrasting spider diagrams. The Group-1 spider diagrams show peaks at Ba, TiO_2, P_2O_5 and Yb, with the overall pattern tilting steeply to the right. The Group-2 spider diagrams exhibit peaks at Rb, Ba, Ce, Zr, Hf, Sm and Y, and troughs at Nb and P_2O_5 (Fig. 8c).

The Geleba calc-alkaline rocks exhibit spider diagrams that tilt to the right, even more steeply than those of the Geleba Group-1 tholeiites. They also show troughs at the positions of Sr, Nb, and Y. Less marked peaks are exhibited at the positions of Ce, Sm and Yb (Fig. 8c).

Moyale tholeiites

The spider diagrams for the Moyale tholeiites fall into two groups (Fig. 8d). Group-1 has an overall higher abundance of trace elements than Group-2 and flat HFS element patterns with only a Rb peak and a trough for K_2O. Group-2 has lower overall trace element abundances and is relatively differentiated compared to the Group-1 patterns. Moreover, the Group-2 patterns tilt to the right, with troughs at K_2O, Zr, Hf, and Sm and, less commonly, at Yb and Th, and peaks at the Ba, Nb, and TiO_2 positions. A single sample of relatively higher TiO_2 (2.4 wt%) exhibits a pattern different from the other Group-2 patterns with troughs at the P_2O_5, Zr, Sm and Y positions.

The Bulbul and Jimma-El Kur rocks show overall higher trace element abundances compared to the Moyale tholeiites (Fig. 8e) and display strongly differentiated patterns. The Bulbul tholeiites have troughs at Nb and peaks at the Ba and Ce positions. The coarse-grained gneissose amphibolite interlayered with high-grade Arero quartzofeldspathic gneisses in the southern part (Arero area) of the Adola granite-gneiss complex shows a pattern similar to those of the Bulbul rocks (Fig. 8e).

The HFS element variations exhibited by the tholeiitic rocks in southern Ethiopia are characteristic of a supra-subduction zone (SSZ) setting, where boninitic and tholeiitic magma mixing could occur (Pearce et al., 1984).

Boninites

Spider diagrams for boninitic rocks, which occur associated with low-Ti tholeiites (LOTI) in the different belts, show more or less similar patterns (Fig. 8f-i). Most boninites have troughs at P_2O_5 and TiO_2, a less pronounced trough at Nb, marked peaks at Ba, Ce, and Sm, and a very strong peak at the Cr position. The Zr, Y, and Sm spidergrams are variable with some samples showing troughs and others peaks. The spider diagrams for the Geleba boninites tilt to the right, with highly normalised values for Cr, resulting in a U-shaped pattern. They show troughs at K_2O, Ba, P_2O_5, and Y, and peaks at Rb, Nb, Zr and TiO_2.

The most distinctive features exhibited by the spider diagrams of the low-Ti tholeiites (LOTI) are the selective enrichments of certain elements (Sr, Ba, Ce, Sm) and the relative lack of enrichment of others (K, P, Zr, Ti, ± Y). These patterns are very similar to those of oceanic basalts from supra-subduction zone (SSZ) settings (Pearce et al., 1984). However, the LOTI and boninitic suites of the study area show enrichment in Yb when compared to similar rocks associated with SSZ settings (e.g., Pearce et al., 1984; Crawford et al., 1989). The Megado tholeiites display spider diagrams resembling those of E-MORB, although the Megado rocks show relatively stronger differentiation and lower overall abundance, especially with respect to their HFS elements. The Megado mafic suite shows stronger selective enrichment than the Geleba mafic suite. The spider diagrams for some of the Moyale tholeiites do not display selective enrichment, especially with respect to the HFS elements and, overall , resemble the spider diagrams of oceanic SSZ tholeiitic basalts from South Sandwich Island (Pearce et al., 1984), except for their slightly higher chondrite-normalised abundance of HFS elements. On the other hand, the boninites and some of the low-Ti tholeiites of Moyale show selective enrichment of their HFS elements and have lower overall trace element concentrations.

The spider diagrams of the high-K Jimma-El Kur and Geleba calc-alkaline rocks show similarity to those of the high-K calc-alkaline SSZ basalts from the New Hebrides (Pearce et al., 1984).

The differential enrichment of the trace elements in the SSZ basalts is interpreted as an effect of subduction. Their characteristics can be attributed to the modification of the mantle source region by a "subduction component" enriched in aqueous and siliceous fluids derived from the underlying subduction zone responsible for the generation of island-arc basalts (Pearce et al., 1984; Best, 1975; Hawkesworth et al., 1977; Saunders and Tarney, 1979).

PETROGENESIS

The geochemical characteristics of the southern Ethiopian mafic suites can be used to evaluate fractional crystallisation processes and implications for the petrogenesis of these basic magmas. An understanding of the fractional crystallisation processes and the genesis of parental magma can, in turn, be used to infer the tectonic setting in which the mafic suites were generated.

As shown in the preceding section, the inter-element correlations among the REE, Zr, Ti, and Hf are similar to those of oceanic basalts (Cann, 1970). These chemical variations may be largely explained by fractional crystallisation of olivine, plagioclase and clinopyroxene and, possibly, orthopyroxene, as is also suggested by decreasing Ni, Cr and V as the REE, Hf, and Zr increase. Fractional crystallisation of plagioclase is also possible, judging from the Eu anomalies observed in the REE patterns. The REE data can be more usefully employed to comment on the petrogenesis of the mafic suites.

The relative changes in Ce_N/Sm_N and Sm_N (Fig. 9) can be explained by fractional crystallisation of mainly pyroxenes (Venturelli et al., 1979, 1981). Figure 9 shows selected inter-element variation diagrams, which indicate differentiation trends when compared with the vectors for various crystallising minerals (e.g., Venturelli et al., 1979, 1981). The Megado and Geleba rocks exhibit two differentiation trends. The vector with the steeper slope shows a differentiation trend similar to the orthopyroxene trend, suggesting accumulation of mainly orthopyroxene in the boninites and associated rocks. In contrast, the other trend has a gentler slope suggesting accumulation of mainly clinopyroxene (Fig. 9). The trends exhibited in these plots rule out the possibility of involvement of olivine and plagioclase in the fractionation of

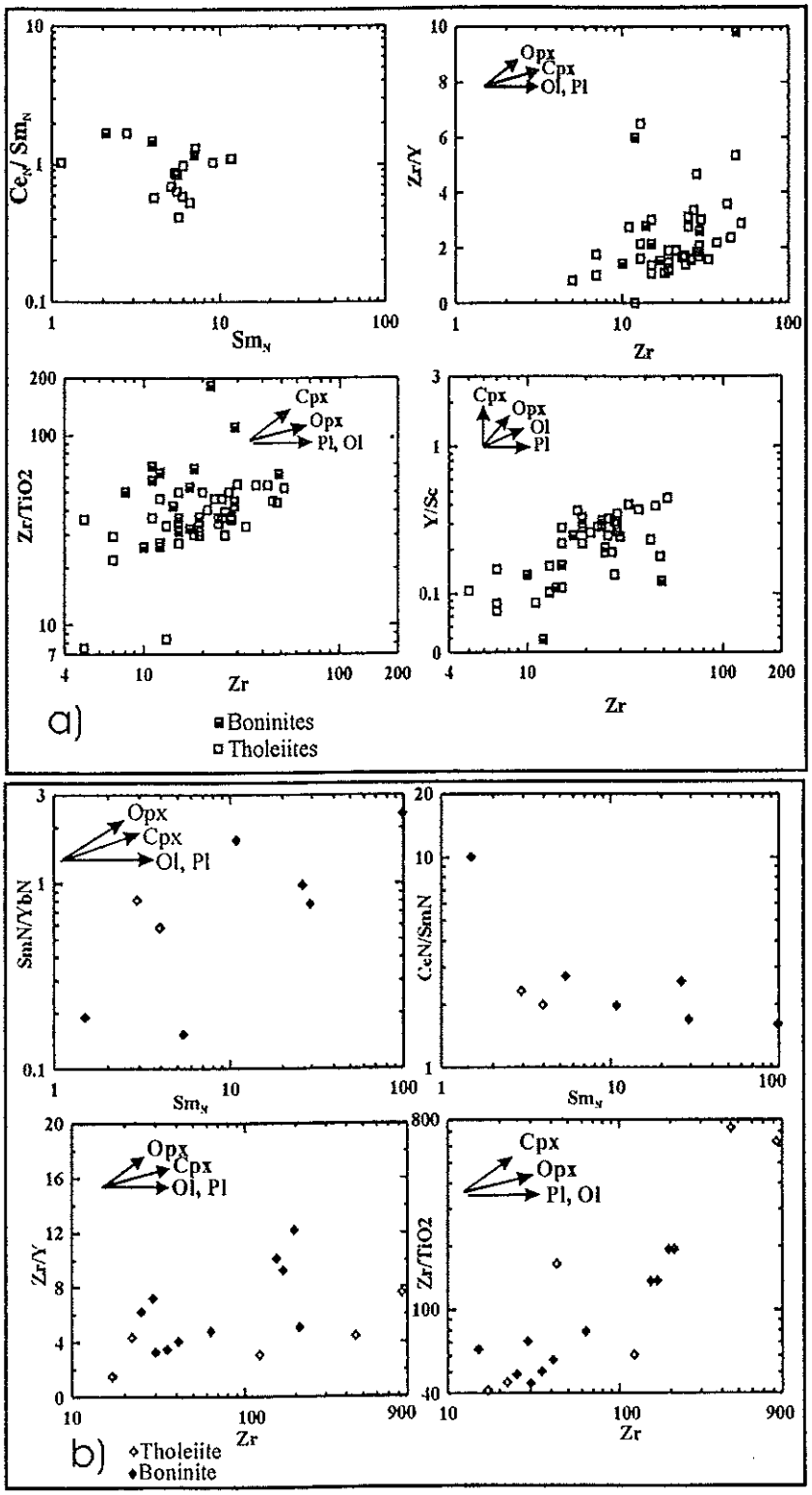

Figure 9: Plots of selected elemental ratios against Sm and Zr to decipher petrogenesis of the Precambrian metabasic rocks of southern Ethiopia: a) Megado, b) Geleba, c) Moyale, Bulbul and Jimma rocks; vectors show differentiation trends of the elemental ratio for selected minerals, after Venturelli et al. (1979). OPX = orthopyroxene, Cpx = clinopyroxene, Ol = olivine, Pl = plagioclase.

Figure 9 (Contd.)

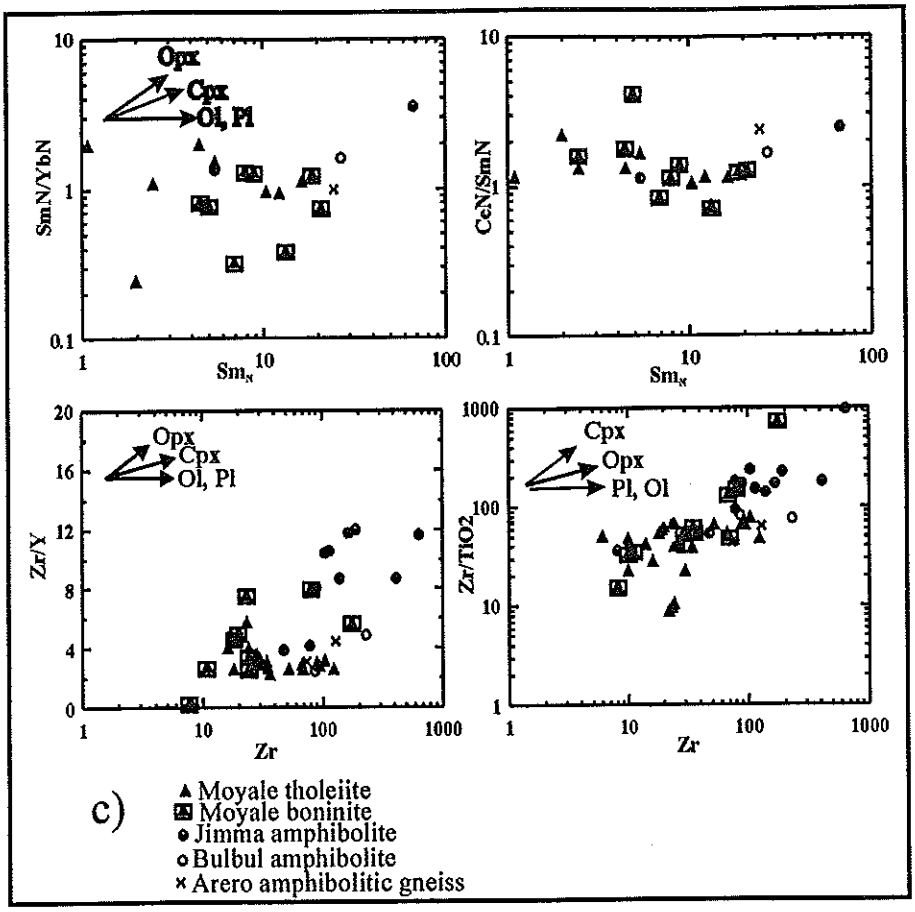

the Megado and Geleba suites. Figure 9 also shows the Ce_N/Sm_N and Sm_N/Yb_N vs. Sm_N plots for the Moyale mafic suite. The diagram shows a differentiation path vector that defines a gentle slope, similar to the differentiation paths of orthopyroxene, plagioclase and olivine. The accumulation of olivine during the differentiation of the Moyale mafic suite is evident, especially in the Ce_N/Sm_N vs. Sm_N diagram (Fig. 9).

The Zr/Y-Zr plot shows the presence of two possible trends: the first has a moderate slope and is similar to the orthopyroxene differentiation trend, whereas the other is more gentle, similar to the plagioclase and olivine differentiation trends (Fig. 9). The Zr/TiO_2-Zr plot, however, displays a trend with a moderate slope, similar to that of the orthopyroxene trend.

According to the boninite classification of Crawford et al. (1989), the Megado boninites are dominantly high Ca-boninites ($SiO_2 < 56$ wt%, $CaO/Al_2O_3 > 0.75$ wt%, total alkalis < 2 wt%, $CaO > 9$ wt%, and $FeO > 7$ wt%). The Megado rocks, in contrast, are characterised by very low Zr values (Yibas, 1993; Wolde et al., 1996; this study). Wolde et al. (1996) suggested that mixing of tholeiitic and boninitic magmas might have resulted in elevated Ti/Zr ratios in some of the Megado boninites. The high-magnesian andesites from Moyale can be classified into two distinct groups. About 50 % of the samples exhibit chemical similarities to high-Ca boninites. The rest of the high-magnesian andesites show high CaO contents (> 12.5 wt%), FeO_T between 7 and 9 wt%, $CaO/Al_2O_3 > 7$ wt%, and total alkali element contents ≤ 1.5 wt%. These findings are characteristic of anhydrous second-stage melts which are commonly found as melt inclusions in MORB (Crawford et al., 1989). Considering the MORB nature of the Moyale tholeiitic rocks and the field relationship of these high-magnesian andesites with tholeiitic basalts, it is plausible that these rocks may be melt inclusions in MORB. This implies

that these rocks are second-stage melts formed at 1275-1300 ^{0}C and $\leq$10kbar conditions (Crawford et al., 1989), from which the Moyale MORB rocks could have been generated.

Although distinct from typical orogenic andesites, boninites as near-primary subduction-related magmas are extremely important as indicators of mantle composition beneath fore-arcs (Sun and Nesbitt, 1977; Jenner, 1981; Hickey and Frey, 1981; Cameron et al., 1983). The relatively low-pressure, high-temperature, hydrous melting conditions inferred from experimental studies (Green, 1976; Tatsumi, 1981, 1982) restrict boninite generation to the uppermost mantle (< 45 km), whereas tholeiitic basalts may be generated at comparatively greater depths or lower P_{H2O}. Therefore, comparison of the trace-element compositions of boninites and tholeiitic lavas from the same area can yield information about the compositional variation within the sub-arc mantle. In this respect, lavas compositionally transitional to boninites are particularly important. Such magmas could originate by melting under temperature and pressure conditions intermediate between those appropriate for boninitic and tholeiitic basalt, and by melting of a relatively fertile rather than harzburgitic mantle, or by mixing of boninite and tholeiitic magmas (Hickey-Vargas, 1989). Wolde et al. (1996) proposed tholeiite-boninite magma mixing for the formation of tholeiites transitional to boninites in the Adola area.

Boninite sources are considered more refractory than the sources for MORB or typical arc basalts because of one or more prior melt extraction events. Invasion of these depleted harzburgites by hydrous fluids, thought to be derived from a subducted slab, could lead to enrichment in large-ion lithophile (LIL) elements, including LREE and Zr and, importantly, also in Na_2O and SiO_2. Two key ingredients for boninite production include : (1) a supply of hydrous fluids into refractory peridotite to lower the solidus temperatures and permit partial melting; and (2) a mechanism for the maintenance of very high temperatures (1150-1350 °C) at shallow levels (< 50 km) in a subduction-zone environment (Crawford et al., 1989).

Crawford et al. (1989) further suggested that the most likely mechanism for generating boninites is subduction of an active spreading centre subparallel to a trench fronting an intra-oceanic arc. They also showed that continued influx of hydrous fluids, and partial melting of increasingly refractory, but increasingly hydrous (and Na-, Si- and LILE-rich) harzburgites might generate a spectrum of boninitic magmas from initial high-Ca boninites to low-Ca boninites sequentially from supra-subduction-zone peridotite. High-Ca boninites could be formed as the hot lithosphere on either side of the spreading centre approaches the trench, and the dip of the slab probably decreases and isotherms in the mantle wedge rise, causing partial melting of depleted sub-fore-arc oceanic lithosphere. Magmatism on the adjacent arc may be terminated due to a change in dip of the slab and the possible interruption of the supply of hydrous fluids from the slab to the site of "normal" arc magma generation at depths of ~100 km. As subduction continues, boninites generated change composition from high-Ca boninites to low-Ca boninites and become more refractory (low TiO_2, CaO, CaO/Al_2O_3, Sc and very low HREE). The increase in temperature required to generate low-Ca boninites is probably due to arrival of the subducted spreading centre beneath the fore-arc.

Crawford et al. (1989) argued that the MORB-type magmatism derived from the spreading centre, as it commences descent along the now very shallowly dipping subduction zone, need not necessarily cease, thereby maintaining high temperatures at shallow levels. MORB-type magmas in shallow magma chambers below the subducted spreading centre may erupt contemporaneously with and after highly depleted type-1 low-Ca boninites, as at Howqua in Victoria (Crawford and Keays, 1987).

If the fore-arc is under tensional stress, as in the modern Mariana-Bonin and Tongan arcs, continued spreading might lead to the splitting of the fore-arc sliver off the mantle wedge leading to a 'resurrection' of 'back-arc-type' spreading in a fore-arc setting and the cessation of boninitic magmatism. The thick tholeiitic pile above boninites in the Victorian Cambrian greenstone belts and in the Betts Cove ophiolite in Newfoundland might have been produced in this manner (Crawford et al., 1989).

Based on this argument, Crawford et al. (1989) suggested that a spectrum of boninitic magmas could be generated sequentially from initial high-Ca boninites to low-Ca boninites from supra-subduction-zone peridotite by continued influx of hydrous fluids and partial melting of increasingly refractory, but increasingly hydrous (and Na-, Si- and LIL-rich) harzburgites. The heat source for the high-temperatures required to allow continued melting in this fashion could be either a MORB-source diapir rising beneath the arc or a subducted active spreading centre. In the latter case, the subducted spreading ridge may be 'resurrected' to yield 'back-arc-basin-type' tholeiites overlying the most refractory boninites, but in a fore-arc setting. Such a scenario is believed to explain the sequence of magma types in several important boninite- and tholeiite-bearing ophiolite belts.

TECTONIC SETTING

The interpretation of the tectonic setting of a metamorphosed and deformed terrain, such as that of southern Ethiopia, is fraught with difficulties. The volcanosedimentary-ultramafic belts of this region suffered metamorphism of up to greenschist-amphibolite transition facies (Beraki et al., 1989; Yibas, 1993; Worku, 1996). This undoubtedly affected the chemistry of the LIL elements (such as K, Ba, Rb and Sr) in particular, which are highly mobile during metamorphism. Therefore, the interpretation of the tectonic setting for the region should, to a large extent, depend on elements of high ionic potential such as Ti, Zr, Cr, and Y, as these elements are effectively immobile during metamorphism (Cann, 1970) and have been proven as such in an earlier section.

A first group of discrimination diagrams uses Ti, Zr, Y, and Sr and was developed by Pearce and Cann (1973). These authors recommended that the Ti-Zr-Y, Ti-Zr, Ti-Zr-Sr diagrams be used together, but should be applied to tholeiitic basalts in the composition range of 20 wt% > CaO+MgO <12 wt%. Therefore, prior to plotting the data on these diagrams, the alkali-basalts are screened using their Y/Nb ratios (Y/Nb < 1 for alkali ocean-island and alkali continental basalts; and Y/Nb < 2 for ocean-floor alkali basalts, see also Fig. 10), which effectively discriminates alkali and tholeiitic basalts.

The Ti-Zr-Y diagram (not shown here) most effectively discriminates between within-plate basalts (WPB), (i.e., ocean-island or continental flood basalts), and other basalt types, namely island-arc tholeiites (IAT) and calc-alkaline basalts (CAB). With the exception of the gneissose amphibolite samples, which are interlayered with high-grade granitic gneisses, the metabasic rocks of southern Ethiopia fall into the CAB, IAT and MORB fields. The Ti-Zr diagram (Fig. 11a) has three fields for MORB, CAB and IAT, respectively, and a fourth field where these three groups overlap. Most of the Megado and Moyale tholeiites and boninites plot into the IAT field. Nevertheless, a few of the Megado samples plot into the overlap field, whereas a few of the Moyale samples show MORB affinity.

The samples from the Bulbul Belt show calc-alkaline affinity. The gneissose amphibolites plot off the edge of the MORB field due to their high Ti and Zr values. The most important

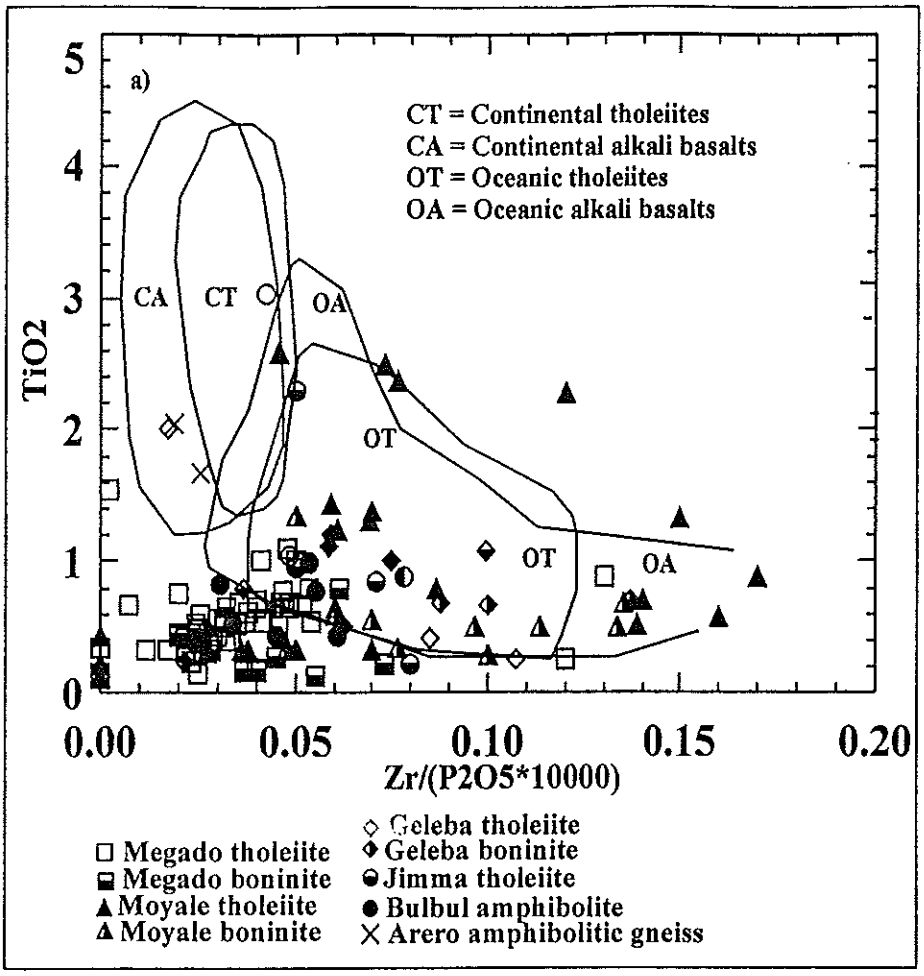

Figure 10: Zr/P_2O_5 - TiO_2 plot to discriminate between oceanic and continental, and alkali and tholeiitic basalts. Diagram after Floyd and Winchester (1971).

inference drawn from this diagram is the absence of MORB basalts amongst the Megado rocks and their limited presence amongst the Moyale tholeiites.

Those samples, which fall into field (B) of the Ti-Zr-Y and Ti-Zr diagrams, either belong to the MORB field or may be part of the oceanic-arc field. In order to differentiate the samples of MORB affinity from those of volcanic-arc affinity, the Ti-Cr diagram (Fig.11b) after Pearce (1975) is useful (Pharaoh and Pearce, 1984). Whereas most of the Megado tholeiites and boninites fall into the IAT field, the Moyale tholeiites and boninites fall either into the ocean-floor basaltic (OFB) field or straddle the boundary of the two fields. The Geleba rocks of southern Megado straddle the boundaries of the two fields, whereas most of the Bulbul and the Jimma-El Kur rocks fall into the island-arc field.

Caution should be observed with regard to those samples plotting and to the left of the discrimination boundary between the MORB and island-arc fields. The position of this boundary depends on whether partial melting occurred recently or during the Proterozoic. If it occurred during the Proterozoic, partial melting may have been stronger than at present, and the discrimination boundary would shift to the left of that shown in the diagram. Therefore, it would be more appropriate to treat the boundary shown on the diagram as the maximum limit of the arc-field (i.e., points plotting just to the left of the boundary may include some MORB samples, provided the partial melting conditions were different during the Proterozoic

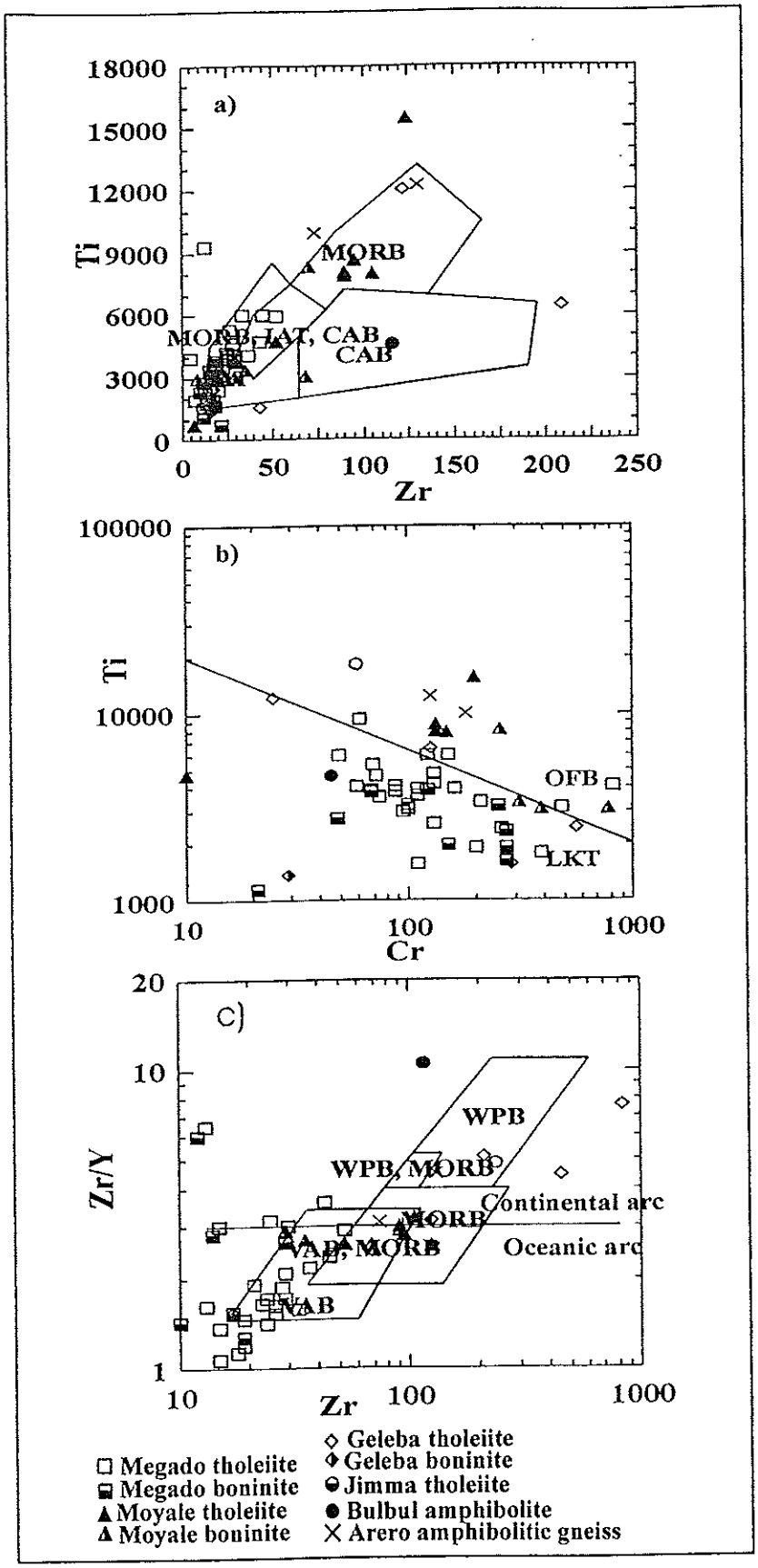

Figure 11: Tectonic discrimination diagrams for the Precambrian metabasic rocks of southern Ethiopia: diagrams after: (a) and (c) Pearce and Cann (1973), (b) Pearce (1975), (d) Shervais (1982), (e) after Pearce et al. (1984) – fore-arc and back-arc fields modified, (f) Mullen (1983).

Figure 11 *(Contd).*

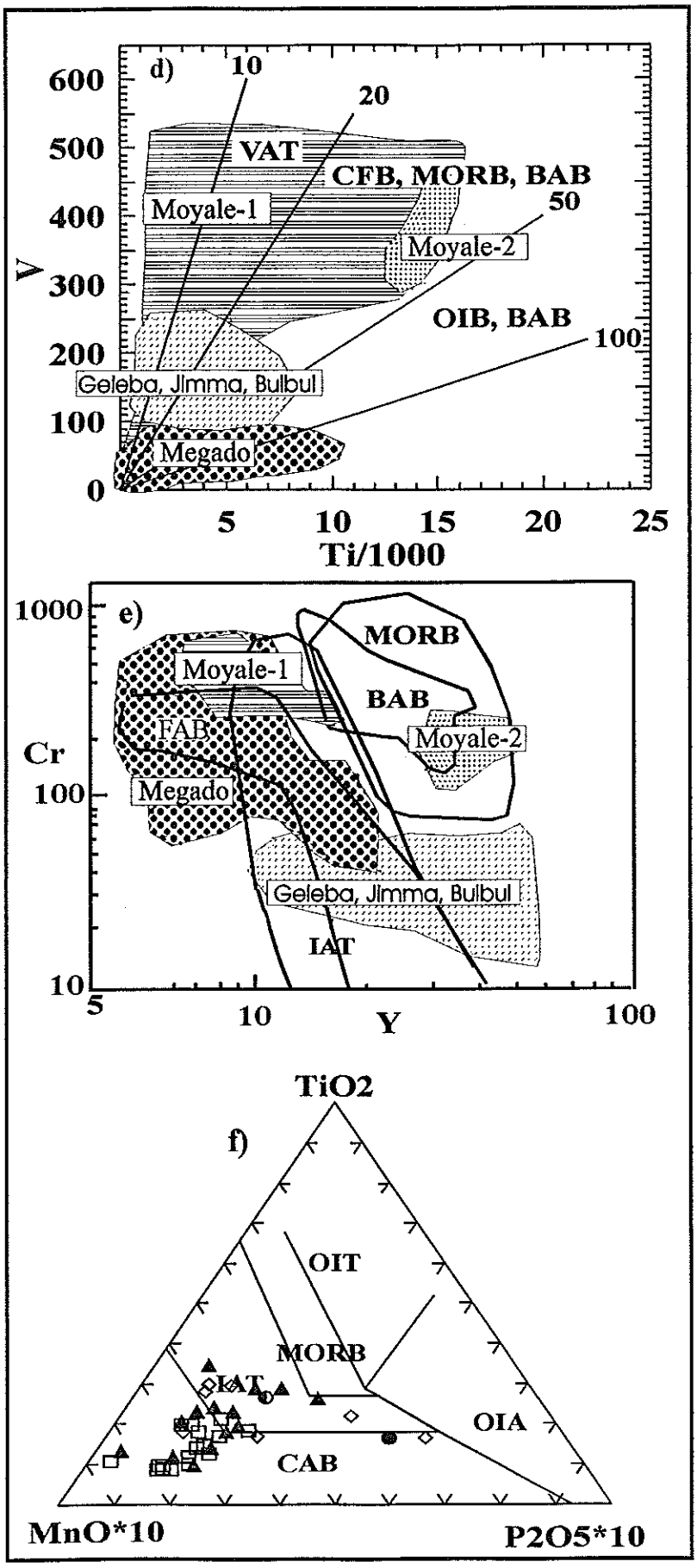

(Pharaoh and Pearce, 1984). Considering this argument, it can be concluded that the Moyale and Geleba rocks show more MORB than island-arc affinity.

Since the introduction of the discrimination diagrams by Pearce and Cann (1973) and Pearce (1975), used above, much has been learned about the chemistry of ocean-floor basalts, and a number of MORB types are now known. Discrimination diagrams that can recognise different types of MORB have been developed (Rollinson, 1993). However, most mafic rocks of the sedimentary-mafic-ultramafic belts of southern Ethiopia show subduction-related affinities, for which further classification can not be achieved by using these discrimination diagrams.

Pearce and Norry (1979) found that the Zr/Y ratio plotted against the fractionation index Zr proved an effective discrimination between basalts from ocean-island arcs, MORB, and within-plate basalts. This diagram can also be used to subdivide the island-arc basalts into oceanic-arcs, where only oceanic crust is used in arc construction, and arcs developed at active continental margins (Pearce, 1983). With the exception of a few samples from the Megado and Bulbul Belts, which show a continental-arc affinity, the entire Moyale suite and the bulk of the Megado rocks show oceanic-arc affinity (Fig. 11c).

In the past 30 years, it has become apparent that there is more than one type of MORB or "ocean-floor basalt", as it was labelled by Pearce and Cann (1973). Meschede (1986) suggested that the immobile trace element Nb could be used to separate different types of ocean-floor basalts into N-MORB (basalt from a 'normal' mid-ocean ridge environment, which is depleted in incompatible trace elements) and E-type MORB (also known as P-type MORB, which represents ocean-floor basalts from plume-influenced regions such as Iceland, which are generally enriched in incompatible trace elements) (Rollinson, 1993). On a triangular Zr/4 - 2Nb -Y diagram, Meschede (1986) showed that four main basalt fields could be identified. Some samples from the Moyale Belt fall into the E-type MORB field, whereas most of the Megado rocks and a few of the Moyale tholeiite samples fall into the fields where volcanic arc and N-type MORB overlap.

The basis of the Ti-V discrimination diagram (Shervais, 1982) is the fact that, although Ti and V are adjacent members of the first transition series in the periodic table, they behave differently in silicate systems. Variation in the concentrations of V, relative to Ti, acts as a measure of oxygen activity of magma and of crystal fractionation processes. These parameters can be linked to the environment of eruption and, thus, can be used for discrimination (Shervais, 1982). Moreover, Ti and V are immobile under conditions of hydrothermal alteration and at intermediate to high grades of metamorphism (Rollinson, 1993). The Megado tholeiites and associated andesites fall into the back-arc basin (BAB) field, where the Ti/V ratio is highest (between 50 and 100, due to the very low absolute V values in these rocks), whereas the Megado rocks fall into the back-arc basin and MORB fields (Fig. 11d). Most boninitic samples from the Moyale Belt fall into the volcanic-arc tholeiitic field, where the V/Ti ratio is between 10 and 20.

The Cr-Y diagram (Pearce, 1982) is important for the discrimination of IAT from MORB rocks. Low concentrations of Cr in volcanic-arc basalts relative to other basalt types have been used in a number of discrimination diagrams to help characterise volcanic-arc basalts (Pearce and Gale, 1977; Garcia, 1978; Bloxham and Lewis, 1972). The low levels of Cr in volcanic-arc rocks represent either a different amount of mantle melting and/or a difference in the fractionation history. Yttrium is also depleted in island-arc basalts relative to other basalt types, for a given degree of fractionation. Thus, a Cr-Y plot (Fig.11e) discriminates effectively between MORB and volcanic-arc basalts. The wide range of Cr values in volcanic-arc basalts is obtained through crystal fractionation (Rollinson, 1993). Besides discriminating between

MORB and arc tholeiites, this diagram has been used to discriminate between different marginal basin rocks. Pearce et al. (1984) plotted the compositional fields for some marginal basin basalts on this diagram and tested its usefulness in discriminating between true oceanic floor basalts and those of marginal basin origin (i.e., fore-arc and back-arc basins). Most back-arc basins fall entirely into the MORB field, whereas those from fore-arc basins (FAB), such as the Mariana fore-arc basins, plot into or to the left of the IAT field (Fig. 11e). Moreover, those samples which fall into the FAB field exhibit boninitic characteristics, and the geochemical characteristic of the basalts, which fall into the BAB field, represent the best analogues for supra-subduction zone ophiolites.

Over 90 % of the data from mafic rocks of southern Ethiopia fall into the FAB and IAT fields. Only two samples from the Moyale suite fall into the BAB field, and a few into the MORB field (Fig. 11e). This indicates that the tectonic setting of the ophiolites of southern Ethiopia is more akin to a fore-arc basin setting than to a back-arc basin or MORB setting.

Basalts and basaltic andesites in the 45-54 wt% silica range can be subdivided on the basis of their MnO, TiO_2 and P_2O_5 concentrations into MORB, ocean-island tholeiites (OIT), ocean-island alkali basalts (OIA), island-arc tholeiites (IAT) and calc-alkali basalts (CAB) (Mullen, 1983). The boninite field occupies the MnO-rich sector of the CAB field. The Moyale MORB tholeiites straddle the boundary of the IAT and MORB fields due to the higher MnO concentration in these rocks. Most boninites of the Moyale Belt fall into the IAT field, whereas the Megado boninites and associated andesites fall into the boninite field (Fig. 11f). The Bulbul and Geleba mafic rocks fall into the island-arc tholeiite (IAT) field.

The tectonic discrimination diagrams discussed enable the recognition of three geochemically distinct mafic suites: (1) Suite-1 (Megado and Moyale-1); (2) Suite-2 (Moyale-2); and (3) Suite-3 (Geleba and Jimma mafic rocks), which can be correlated with IAT-FAB, MORB-BAB, and IAT tectonic settings, respectively (Figs. 11d , e).

DISCUSSION AND CONCLUSIONS

Subalkaline, low-K, low-Ti (LOTI) tholeiitic basalts, with minor amounts of andesitic basalts and andesites, are the most dominant mafic rocks in the low-grade belts of the Precambrian of southern Ethiopia. Low P_2O_5 and Zr values and the increase in Ti with increase of Zr further corroborate the dominance of tholeiitic basaltic rocks. The Y and Nb values of a few samples, mainly from the Moyale mafic suite, are similar to alkali basaltic rocks of both oceanic and continental affinity. However, the Y/Nb ratio could also be lower due to possible crustal contamination of mantle-derived magmas (e.g., Wilson, 1989). Minor occurrences of high-K calc-alkaline lavas within the belts of Bulbul, Geleba (southern Megado) and Jimma-El Kur have been recognised. A few samples from each belt fall into the alkali basaltic field, as seen in Figures 6a and b.

The present study shows widespread occurrence of boninitic magmatism in association with low-Ti tholeiites in the sedimentary-mafic-ultramafic assemblages of southern Ethiopia, with the exception of the Bulbul Belt. The petrogenesis of the boninites of the Moyale Belt shows a likely association with second-melt inclusions in the MORB of Moyale, which might indicate a somewhat different tectonic setting for the Moyale ophiolites from that of the Megado ophiolites, where the boninites are dominantly high-Ca boninites with lesser second-melt inclusions.

The REE patterns of the Moyale tholeiites are distinctly different from those of the Megado tholeiites. The Moyale tholeiites have higher REE abundances, especially higher Ce

concentrations, and their positive Eu anomalies die out with increasing differentiation. The Megado tholeiites also have strong LREE depleted patterns unlike the Moyale tholeiites, which have moderate LREE enrichment. The Moyale REE patterns are more similar to N-MORB patterns, whereas those of Megado samples are similar to more evolved oceanic tholeiites and back-arc tholeiites.

The most distinctive features exhibited in the spider diagrams of the low-Ti (LOTI) tholeiites include the selective enrichment of certain elements (Sr, Ba, Ce, Sm) and the relative lack of enrichment for others (K, P, Zr, Ti, $\pm$ Y). These patterns are very similar to those of oceanic basalts from SSZ settings (Pearce et al., 1984). However, the LOTI and boninitic suites of the study area show enrichment in Yb when compared to many similar rocks associated with SSZ settings. The Megado tholeiites show spider diagrams that resemble those of E-MORB, although the Megado rocks show relatively stronger differentiation and lower overall abundances, especially with respect to their HFS elements.

The Bulbul and Jimma-El Kur tholeiites are more alkaline than their counterparts in the Moyale and Megado Belts. Moreover, these rocks consistently fall into calc-alkaline basaltic fields on the various discrimination diagrams, suggesting that they may represent a mature island-arc setting when compared to the Megado and the Moyale mafic suites. The spider diagrams of the high-K Jimma-El Kur, Geleba and Bulbul calc-alkaline rocks show similarity with those of high-K New Hebrides calc-alkaline SSZ basalts.

The geochemical characteristics permit inferences about the tectonic setting of the low-grade sedimentary-mafic-ultramafic belts of southern Ethiopia. Close study of the various discrimination plots, especially Figures 11d and e, reveal that the Megado mafic rocks are more akin to fore-arc basin (FAB-IAT) mafic suites than the Moyale rocks. The Moyale mafic rocks can be classified into Moyale-1, which shows transitional geochemistry between the IAT and MORB-BAB) rock suites, and a minor group (Moyale-2) of MORB-BAB affinity with no IAT signature. The Megado and Moyale-1 suites show stronger subduction characteristics than the Moyale-2 Suite. This is also supported by the relatively lower concentrations of most of the immobile elements (such as Ti, Nb, P, Ce, Zr, Th and V) in the Megado and Moyale-1 suites as compared to the Moyale-2 Suite. The Geleba and Jimma mafic rocks show transitional geochemical characteristics between the Moyale and Megado suites

The association of high Ca-boninites and second-melt inclusions with the low-tholeiite (LOTI) rocks (Crawford et al., 1989) further corroborates that the Megado, Moyale and Jimma-El Kur ophiolitic assemblages were formed in a supra-subduction zone (SSZ) setting. The geochemistry of the Bulbul mafic rocks indicates formation in a mature island-arc setting.

The geochronological order in which the different ophiolites were formed in southern Ethiopia is becoming clearer as a result of recent geochronological work. The 700 Ma U-Pb zircon age obtained for the amphibolitic rocks from the Moyale ophiolitic fold and thrust belt by Teklay et al. (1998) has been interpreted as an approximation of their formation age. The formation age of the Megado ophiolite is approximately 789$\pm$36 Ma (Sm-Nd whole-rock isochron age for the Megado metavolcanics, Worku, 1996). The 876$\pm$5 Ma (U-Pb, zircon SHRIMP age, Yibas et al., 2000b) obtained for the Bulbul dioritic mylonite gneiss from the Bulbul Belt implies the presence of an early- or pre-Pan African ocean in southern Ethiopia (Yibas, 2000). It is plausible that the Kenticha and Bulbul ophiolites may represent the same pre-880 Ma ocean, which was perhaps the oldest Pan–African ocean in southern Ethiopia.

ACKNOWLEDGEMENTS

This paper has resulted from the PhD project by Bisrat Yibas, which benefited from generous financial support from Anglo American Prospecting Services, Johannesburg. Sharon Farrell of the Geology Department, University of the Witwatersrand is thanked for carryimng out the XRF major element analyses. Richard Holdsworth and his group at the Anglo American Research Laboratory (AARL), Johannesburg, are thanked for the ICP-MS trace element analyses.

REFERENCES

Abu El-Ela, F.F., 1996. The petrology of the Abu Zawal gabbroic intrusion, eastern Desert, Egypt: an example of an island-arc setting. J. Afr. Earth Sci., **22**, 147-157.

Beraki, W.H., Bonavia, F.F., Getachew, T., Schmerold, R. and Tarekegn, T., 1989. The Adola fold and thrust belt, southern Ethiopia: a re-examination with implications for Pan-African evolution, Geol. Mag., **126**, 647-657.

Best, M., 1975. Amphibole-bearing cumulate inclusions, Grand Canyon, Arizona, and their bearing on silica-undersaturated hydrous magmas in the upper mantle. J. Petrol., **16**, 212-236.

Bloxham, W. and Lewis, A.D., 1972. Ti, Zr, and Cr in some British pillow lavas and their petrogenetic affinities. Nature (Phys. Science) **237**, 134-136.

Cameron, W. E., 1989. Contrasting boninites-tholeiite associations from New Caledonia. In: Crawford, A. J. (Ed.), *Boninites*. Unwin Hyman. London, pp. 314-338.

Cameron, W.E., McColluch, M.T. and Walker, D.E., 1983. Boninite petrogenesis: chemical and Nd-Sr isotopic constraints. Earth Planet. Sci. Lett., **65**, 75-89.

Cann, J.R., 1970. Rb, Sr, Y, Zr, and Nb in some ocean-floor basaltic rocks. Earth Planet. Sci. Lett., **10**, 7-11.

Crawford, A.J. and Keays, R.R., 1987. Petrogenesis of Victorian Cambrian tholeiites and implications for the origin of associated boninites. J. Petrol., **91**, 93-104.

Crawford, A.J., Falloon, T.J. and David, H.G., 1989. Classification, petrogenesis and tectonic setting of boninites. In: Crawford, A. J. (Ed.), *Boninites*. Unwin Hyman, London, pp. 2-44.

De La Roche, H., 1978. La chimie des roches présentée et interprétée d'après la structure de leur facies minèral dans l'espace des variables chimiques: fonctions spécifiques et diagrammes qui s'en déduisent. Application aux roches ignèes. Chem. Geol., **21**, 63-87.

Floyd, P.A. and Winchester, J.A., 1971. Magma type and tectonic setting discrimination using trace elements. Earth Planet. Sci. Lett., **27**, 211-218.

Frey, F.A., 1983. Rare earth element abundances in upper mantle rocks. In: P. Henderson (Ed.), *Rare Earth Element Geochemistry*. Elsevier, Amsterdam, pp. 256-259.

Frey, F.A. and Green, D.H., 1974. The mineralogy, geochemistry and origin of lherzolite inclusions in Victorian basanites. Geochim. Cosmochim. Acta **38**, 1023-1059.

Frey, F.A., Green, D.H. and Roy, S.D., 1978. Integrated models of basalt petrogenesis: a study of quartz tholeiites to olivine melilites from southeastern Australia utilising geochemical and experimental petrological data. J. Petrol., **19**, 463-513.

Garcia, M.O., 1978. Criteria for the identification of ancient volcanic areas. Earth Planet. Sci. Lett., **14**, 147-165.

Green, D.H., 1976. Experimental testing of "equilibrium" partial melts of peridotite under water-saturated, high-pressure conditions. Can. Mineral., **14**, 255-268.

Hawkesworth, C.J., O'Nions, R.K., Pankhurst, R.J., Hamilton, P..J. and Evensen, N..M. ,1977. A geochemical study of island-arc and back-arc tholeiites from Scotia Sea. Earth Planet. Sci. Lett., **36**, 253-262.

Hickey, R.L. and Frey, F.A., 1981. Rare earth element geochemistry of Mariana fore-arc volcanics: deep Sea Drilling Project Site 458 and Hole 459B. Init. Rep. DSDP Leg, 60, 735-742.

Hickey-Vargas, R., 1989. Boninites and tholeiites from DSDP Site 458, Mariana fore-arc. In: Crawford A.J. (Ed.), *Boninites*. Unwin Hyman, London, pp. 340-354.

Hughes, C.J., 1973. Spilites, keratophyres, and the igneous spectrum. Geol. Mag., **109**, 513-527.

Irvine T.R. and Baragar, W.R .A., 1971. A guide to the chemical classification of the common volcanic rocks. Can. J. Earth Sci., **8**, 523-548.

Jenner, G.A., 1981. Geochemistry of high-Mg andesites from Cape Vogel, Papua, New Guinea. Chem. Geol., **33**, 307-332.

Koeberl, C. 1993. Instrumental neutron activation analysis of geochemical and cosmochemical samples: a fast and proven method for sample analysis. J. Radioanal. Nucl. Chem., **168**, 47-60.

Koeberl, C., Kluger, F. and Kiesl, W., 1987. Rare earth element determinations at ultra-trace abundance levels in geologic materials. J. Radioanal. Nucl. Chem., **112**, 482-487

Meschede, M., 1986. A method of discrimination between different types of mid-oceanic ridge basalts and continental tholeiites with the Nb-Zr-Y diagram. Chem. Geol., **56**, 207-218.

Miyashiro, A., 1975. Classification, characteristics and origin of ophiolites. J. Geol., **83**, 249-281.

Mullen, E.D., 1983. $MnO/TiO_2/P_2O_5$: a minor element discriminant for basaltic rocks of oceanic environments and implication for petrogenesis. Earth Planet. Sci. Lett., **62**, 53-62.

Nakamura, N., 1974. Determination of REE, Ba, Fe, Mg, Na, and K in carbonaceous and ordinary chondrite. Geochim. Cosmochim. Acta **38**, 757-775.

Nelson, D.R., Crawford, A.J. and McCulloch, M.T., 1984. Nd-Sr isotope and geochemical systematics in Cambrian boninites and tholeiites from Victoria, Australia. Contriib. Mineral. Petrol., **88**, 164-172

Pearce, J.A., 1975. Basalt geochemistry to investigate past tectonic environments on Cyprus. Tectonophysics, **25**, 41-67.

Pearce, J.A., 1982. Trace element characteristics of lavas from destructive plate boundaries. In: Thorpe, R.S. (Ed.), *Andesites*. Unwin Hyman, London, pp. 525-548.

Pearce, J.A., 1983. Role of the sub-continental lithosphere in magma genesis at active continental margins. In: Hawkesworth, C.J. and Norry, M. J. (Eds.), *Continental Basalts and Mantle Xenoliths*. Shiva, Nantwich, pp. 230-249.

Pearce, J.A. and Cann, J.R., 1973. Tectonic setting of basic volcanic rocks determined using trace element analyses. Earth Planet Sci. Lett., **19**, 290-300.

Pearce, J.A. and Gale, G.H., 1977. Identification of ore deposit environment from trace element geochemistry of associated igneous host rocks. Spec. Publ. Geol. Soc. Lond., **7**, 14-24.

Pearce, J.A. and Norry, M.J., 1979. Petrogenetic implications of Ti, Zr, Y, and Nb variations in volcanic rocks. Contrib. Mineral. Petrol., **69**, 33-47.

Pearce, J.A., Lippard, S.J. and Roberts, S., 1984. Characteristics and tectonic significance of suprasubduction zone ophiolites. In: Kokiaar, B.P. and Howells, M.F. (Eds.), *Marginal Basin Geology*. Spec. Publ. Geol. Soc. Lond., **16**, 77-94.

Pharaoh, T.C. and Pearce, J.A., 1984. Geochemical evidence for the geotectonic setting of early Proterozoic metavolcanic sequence in Lapland. Precambrian Res., **25**, 283-308.

Rollinson, H.R., 1993. *Using Geochemical Data: Evaluation, Presentation and Interpretation*. Wiley, New York, 351pp.

Saunders, A.D. and Tarney, J., 1979. The geochemistry of basalts from back-arc spreading centers in the East Scotia Sea. Geochim. Cosmochim. Acta **43**, 555-572.

Shagi, T., Bonavia, F. F., Meshesha, S. and Eshete, T., 1991. Structural pattern of Pan-African rocks around Moyale, southern Ethiopia. Precambrian Res., **52**, 179-186.

Shervais, J.W., 1982. Ti-V plots and the petrogenesis of modern and ophiolitic lavas. Earth Planet. Sci. Lett., **59**, 101-118.

Sun, S.S. and Nesbitt, R.W., 1977. Chemical heterogeneity of the Archean mantle: composition of the earth and mantle evolution. Earth Planet. Sci. Lett., **35**, 429-448.

Tatsumi, Y., 1981. Melting experiments on a high-magnesian andesite. Earth Planet.Sci.Lett., **54**, 357-65.

Tatsumi, Y., 1982. Origin of high-magnesian andesites in the Setouchi volcanic belt, southwest Japan, II, Melting phase relations at high pressures. Earth Planet. Sci. Lett., **60**, 305-317.

Turner, F. J., 1981. *Metamorphic Petrology: Mineralogical and Field Tectonic Aspects*. New York, McGraw-Hill, 541pp.

Venturelli, G., Capedri, S., Thorpe, R.S., Thorpe, R.S. and Potts, P.J., 1979. Rare earth element and other element distribution in some ophiolitic metabasalts of Corsica, western Mediterranean. Chem. Geol., **24**, 339-353.

Venturelli, G.,Thorpe, R. S. and Potts, P. J.,1981. Rare earth and trace element characteristics of ophiolitic metabasalts from the Alpine-Apennine Belt. Earth Planet. Sci. Lett., **53**, 109-123.

Walsh, J., 1972. Geology of the Moyale area. Ministry of Natural Resources, Geological Survey of Kenya. Degree Sheet 14. Report No. 89, 32pp.

Wilson, M., 1989. *Igneous Petrogenesis: a Global Tectonic Approach*. Unwin Hyman, London, 466pp.

Winchester, J.A. and Floyd, P.A., 1977. Geochemical discrimination of different magma series and their differentiation products using immobile elements. Chem. Geol., **20**, 325-343.

Wolde, B., Asres, Z., Desta, Z. and Gonzalez, J.J., 1996. Neoproterozoic zirconium-depleted boninite and tholeiite series rocks from Adola southern Ethiopia. Precambrian Res., **80**, 261-279.

Woldehaimanot, B. and Behrmann, J. H., 1995. A study of metabasites and metagranite chemistry in the Adola Region (south Ethiopia): implication for the evolution of the east African Orogen. J. Afr. Earth Sci., **21**, 459-476.

Worku, H., 1996. *Geodynamic development of the Adola Belt (southern Ethiopia) in the Neoproterozoic and its control on gold mineralisation.* Ph.D. thesis (unpubl.), Berlin Tech. Univ., Germany, 156pp.

Yibas, B., 1993. The geochemistry of the metabasic rocks of the Adola volcanosedimentary-ultramafic assemblage: evidence from supra-subduction zone (SSZ) ophiolitic sequence, Adola, southern Ethiopia. Report, Ethiopian Institute of Geological Surveys, Addis Ababa, 18pp.

Yibas, B., 2000. *The Precambrian geology, tectonic evolution, and controls of gold mineralisations in southern Ethiopia.* Ph.D. thesis (unpubl.), University of the Witwatersrand, Johannesburg, 448 pp.

Yibas, B., Reimold, W. U. and Anhaeusser, C. R., 2000a. The geology of the Precambrian of southern Ethiopia: I - The tectonostratigraphic record. Inform. Circ. Economic Geology Research Institute, Univ. Witwatersrand, Johannesburg, **344**, 21pp.

Yibas, B., Reimold, W. U., Armstrong, R., Phillips, D., and Koeberl, C. 2000b. The geology of the Precambrian of southern Ethiopia: II - U-Pb single zircon SHRIMP and laser argon dating of granitoids. Inform. Circ. Economic Geology Research Institute, Univ. Witwatersrand, Johannesburg, **345**, 30pp.

oOo

APPENDIX

Table 1a. Mafic rocks of the Megado Belt

Sample	Dg3643	Dg3645	Dg3647	Dg3648	Dg3649	Dg3651	Dg3652	Dg3654	Dg3655	Dg3656
Major elements (wt%)										
SiO2	41.70	53.50	46.40	48.70	50.70	49.70	49.90	49.20	48.30	54.70
TiO2	0.88	0.65	0.52	0.66	0.65	0.39	0.61	0.39	0.50	0.46
Al2O3	15.50	13.40	13.50	13.00	12.90	13.00	12.90	13.70	15.70	15.00
Fe2O3T	20.30	15.70	17.60	13.60	15.70	16.70	15.30	11.20	14.40	14.20
MnO	0.33	0.20	0.24	0.22	0.24	0.24	0.23	0.19	0.21	0.21
MgO	7.60	5.38	7.70	6.93	6.24	6.24	7.16	8.39	5.86	3.77
CaO	10.00	9.95	11.10	10.50	10.10	10.10	10.50	11.70	11.80	9.12
Na2O	2.02	1.33	1.53	1.50	1.57	1.27	1.93	2.37	1.69	2.06
K2O	0.17	0.20	0.20	0.27	0.34	0.25	0.19	0.13	0.25	0.24
P2O5	0.02	0.09	0.06	0.05	0.06	0.05	0.05	0.04	0.05	0.06
LOI	0.77	0.00	0.00	3.54	1.23	1.00	0.62	1.54	0.54	0.54
TOTAL	99.30	100.00	98.50	99.00	99.70	99.00	99.40	98.90	99.30	100.40
Trace elements (ppm)										
Sc	64.5	41.7	42.4	52.7	47.8	51.7	53.3	52.0	49.3	40.9
V	32	24	39	67	58	40	43	26	36	55
Cr	69	120	480	110	68	270	110	270	95	48
C0	13	19	25	30	27	25	18	17	22	38
Ni	16	37	100	27	28	40	25	19	22	12
Cu	24.9	92.5	178.0	3.3	31.7	138.0	132.0	81.9	40.4	67.6
Zn	23.2	11.2	20.0	41.8	36.4	18.8	18.1	12.7	15.9	30.6
Rb	*	*	*	*	*	*	*	*	*	*
Sr	37	116	122	111	72	104	74	101	96	112
Y	16	11	11	17	14	8	16	7	14	2
Zr	26	29	21	26	24	13	19	10	23	12
Nb	*	*	*	3.0	*	*	*	3.0	*	*
Sb	0.9	2.2	3.6	0.2	0.9	2.7	0.8	0.6	1.0	0.7
Cs	*	*	*	2	*	1	*	*	*	*
Hf	1.3	*	0.8	*	*	*	0.7	*	*	*
Ta	*	1	*	*	1	1	*	*	*	*
W	23	120	49	100	120	120	49	80	81	220
Pb	nd	nd	nd	nd	nd	nd	nd	nd	nd	nd
Th	nd	*	nd	nd	nd	nd	nd	nd	nd	nd
U	nd	0	nd	nd	nd	nd	nd	nd	nd	nd
Ba	98	90	91	76	55	104	61	44	38	51
Rare earth elements (ppm)										
La	nd	2.7	nd	0.8	nd	nd	nd	nd	nd	nd
Ce	nd	7.0	nd	2.0	nd	nd	nd	nd	nd	nd
Pr	nd	nd	nd	nd	nd	nd	nd	nd	nd	nd
Nd	nd	5.0	nd	nd	nd	nd	nd	nd	nd	nd
Sm	nd	1.4	nd	1.1	nd	nd	nd	nd	nd	nd
Eu	nd	0.5	nd	0.6	nd	nd	nd	nd	nd	nd
Gd	nd	nd	nd	nd	nd	nd	nd	nd	nd	nd
Tb	nd	0.3	nd	0.5	nd	nd	nd	nd	nd	nd
Dy	nd	nd	nd	nd	nd	nd	nd	nd	nd	nd
Ho	nd	nd	nd	nd	nd	nd	nd	nd	nd	nd
Er	nd	nd	nd	nd	nd	nd	nd	nd	nd	nd
Tm	nd	nd	nd	nd	nd	nd	nd	nd	nd	nd
Yb	nd	2.0	nd	2.3	nd	nd	nd	nd	nd	nd
Lu	nd	0.3	nd	0.4	nd	nd	nd	nd	nd	nd

Table 1a.(Continued)

Sample	Dg3657	Dg3658	Dg3659	Dg3660	Dg3661	Dg3662	Dg3663	Dg3664	Dg3665	Dg3666
Major elements (wt%).										
SiO2	49.30	47.70	47.70	54.30	47.60	51.40	48.00	52.90	49.20	51.40
TiO2	0.56	0.54	0.99	0.27	1.00	0.64	1.00	0.48	0.43	0.68
Al2O3	12.70	14.00	14.30	12.70	15.00	12.70	12.20	13.40	13.80	15.60
Fe2O3T	19.30	11.50	18.50	11.40	16.60	16.00	21.80	12.40	16.10	12.60
MnO	0.27	0.18	0.27	0.21	0.26	0.24	0.33	0.18	0.24	0.19
MgO	6.60	8.97	3.28	6.08	6.15	6.18	6.43	6.86	6.95	5.70
CaO	9.81	11.20	12.90	9.65	9.83	9.89	9.30	9.55	11.23	9.65
Na2O	1.45	2.51	0.85	2.28	2.17	1.59	1.34	2.91	2.02	3.40
K2O	0.23	0.14	0.26	0.40	0.24	0.34	0.24	0.18	0.19	0.24
P2O5	0.05	0.05	0.10	0.04	0.09	0.06	0.08	0.06	0.05	0.06
LOI	0.00	3.16	1.00	3.00	1.23	1.16	0.00	0.70	0.47	0.31
TOTAL	100.20	100.10	100.20	100.40	100.20	100.20	100.20	99.70	100.70	100.00
Trace elements (ppm)										
Sc	50.1	42.0	40.3	36.0	48.4	47.4	52.1	44.6	50.3	48.8
V	65	39	73	35	59	49	59	35	46	34
Cr	210	1000	120	270	49	87	150	470	130	820
C0	38		45	33	36	32	31	29	38	34
Ni	53	162	38	39	22	29	48	57	52	57
Cu	182.0	91.6	84.1	51.4	48.8	39.0	101.0	105.0	172.0	145.0
Zn	25.8	62.6	36.9	34.8	39.7	28.4	27.7	18.8	25.4	16.4
Rb	*	*	*	3.0	*	*	*	*	*	*
Sr	80	170	214	116	189	72	37	102	64	74
Y	14	8	18		19	14	21	7	11	17
Zr	15	27	52	18	45	29	33	15	15	29
Nb	*	*	2.0	*	*	2.0	*	4.0	3.0	*
Sb	2.9	1.8	2.3	1.6	1.2	1.0	2.6	1.5	2.3	1.1
Cs	1	1	1	2		*	3	*	1	*
Hf	*	0.9	0.9	*	1.8	*	*	*	*	0.8
Ta	*	*	*	*	*	*	*	*	*	2
W	160	75	75	160	130	210	180	110	150	180
Pb	nd	nd	nd	nd	nd	nd	nd	nd	nd	nd
Th	nd	nd	nd	nd	nd	nd	nd	nd	nd	nd
U	nd	nd	nd	nd	nd	nd	nd	nd	nd	nd
Ba	65	91	46	111	79	69	93	99	57	54
Rare earth elements(ppm)										
La	nd	1.1	nd	nd	nd	nd	nd	1.7	nd	nd
Ce	nd	3.0	nd	nd	nd	nd	nd	4.0	nd	nd
Pr	nd	nd	nd	nd	nd	nd	nd	nd	nd	nd
Nd	nd	3.0	nd	nd	nd	nd	nd	3.0	nd	nd
Sm	nd	1.1	nd	nd	nd	nd	nd	1.1	nd	nd
Eu	nd	0.7	nd	nd	nd	nd	nd	0.4	nd	nd
Gd	nd	nd	nd	nd	nd	nd	nd	nd	nd	nd
Tb	nd	0.3	nd	nd	nd	nd	nd	0.3	nd	nd
Dy	nd		nd	nd	nd	nd	nd	nd	nd	nd
Ho	nd		nd	nd	nd	nd	nd	nd	nd	nd
Er	nd		nd	nd	nd	nd	nd	nd	nd	nd
Tm	nd		nd	nd	nd	nd	nd	nd	nd	nd
Yb	nd	1.3	nd	nd	nd	nd	nd	1.5	nd	nd
Lu	nd	0.2	nd	nd	nd	nd	nd	0.2	nd	nd

Table 1a. (Continued)

Sample	Dg3668	Dg3669	Dg3705	Dg3707	Dg3715	DgG3644	DgG3646	Ga3626	Ga3627	Ga3629
Major elements (wt%)										
SiO2	48.50	50.40	50.60	52.30	58.40	50.40	49.30	49.20	50.50	54.40
TiO2	0.39	0.41	0.19	0.21	0.12	0.70	0.68	0.79	0.60	0.64
Al2O3	13.50	15.30	17.00	14.30	6.37	12.20	14.40	13.60	13.50	12.00
Fe2O3T	12.10	15.90	9.68	11.20	10.60	17.90	14.70	12.30	16.40	16.10
MnO	0.20	0.22	0.17	0.17	0.17	0.25	0.23	0.16	0.20	0.22
MgO	9.67	5.04	7.48	8.11	13.70	6.44	5.97	7.43	3.79	5.26
CaO	11.60	10.30	12.50	9.61	6.20	9.99	9.62	12.20	13.60	10.30
Na2O	1.73	1.12	1.47	2.14	0.23	1.40	2.63	2.27	0.52	0.63
K2O	0.23	0.17	0.13	0.27	0.08	0.20	0.18	0.39	0.12	0.14
P2O5	0.04	0.07	0.03	0.03	0.04	0.06	0.08	0.08	0.07	0.04
LOI	1.85	1.23	0.85	1.54	3.31	0.00	1.16	0.47	0.70	0.31
TOTAL	99.90	100.20	100.10	99.90	99.50	99.60	99.00	98.90	100.00	100.10
Trace elements (ppm)										
Sc	59.5	42.4	40.7	40.1	26.9	54.1	45.5	51.4	43.5	45.9
V	38	83	34	31	23	66	36	25	39	40
Cr	330	40	19	325	1920	130	59	130	74	68
C0	15	30	34	35	40	32	14	16	15	73
Ni	25	19	16	33	168	43	21	17	22	43
Cu	18.1	79.3	65.7	130.0	76.6	120.0	61.3	24.5	72.0	211.0
Zn	18.0	44.4	14.3	26.8	29.4	31.0	17.3	6.5	21.0	16.2
Rb	*	*	*	2.0	*	*	*	4.0	*	*
Sr	79	205	101	122	22	59	252	211	106	46
Y	6	*	*	*	*	17	17	12	16	15
Zr	13	15	11	22	22	24	37	43	18	19
Nb	*	2.0	2.0	4.0	3.0	3.0	*	5.0	*	*
Sb	0.4	0.7	*	*	*	1.8	1.5	0.7	1.6	2.1
Cs	2	*	*	*	*	*	*	*	1	*
Hf	*	*	*	*	*	*	*	*	*	1.1
Ta	*	*	*	*	*	*	*	*	*	
W	65	110	230	210	140	110	41	51	72	370
Pb	nd	nd	nd	nd	nd	nd	nd	nd	nd	nd
Th	nd	nd	nd	nd	nd	nd	nd	nd	nd	nd
U	nd	0	nd	nd	nd	0	nd	nd	nd	nd
Ba	124	38	60	210	140	51	56	40	23	87
Rare earth elements (ppm)										
La	0.8	2.1	nd	nd	nd	1.0	4.1	nd	nd	1.0
Ce	2.0	5.0	nd	nd	nd	3.0	11.0	nd	nd	3.0
Pr	nd	nd	nd	nd	nd	nd	nd	nd	nd	nd
Nd	nd	3.0	nd	nd	nd	3.0	7.0	nd	nd	3.0
Sm	0.8	0.8	nd	nd	nd	1.3	2.4	nd	nd	1.2
Eu	0.4	0.5	nd	nd	nd	0.7	1.2	nd	nd	0.6
Gd	nd	nd	nd	nd	nd	nd	nd	nd	nd	nd
Tb	0.3	0.2	nd	nd	nd	0.5	0.6	nd	nd	0.6
Dy	nd	nd	nd	nd	nd	nd	nd	nd	nd	nd
Ho	nd	nd	nd	nd	nd	nd	nd	nd	nd	nd
Er	nd	nd	nd	nd	nd	nd	nd	nd	nd	nd
Tm	nd	nd	nd	nd	nd	nd	nd	nd	nd	nd
Yb	1.4	0.9	nd	nd	nd	2.8	2.6	nd	nd	2.5
Lu	0.2	0.2	nd	nd	nd	0.5	0.4	nd	nd	0.4

Table 1a. (Continued)

Sample	Ga3630	Ga3631	Ga3632	Ga3618	Ga3619	Ga3620	Ga3621	Ga3622	Ga3623	Ga3624
Major elements (wt%)										
SiO2	41.90	48.70	50.90	47.80	50.90	47.40	48.50	49.50	48.80	49.40
TiO2	1.09	0.54	0.33	0.13	0.53	0.78	0.14	0.51	0.24	0.32
Al2O3	14.70	14.00	14.40	14.10	13.30	13.00	12.20	13.70	14.60	13.20
Fe2O3T	18.20	14.90	13.40	13.80	14.70	18.10	12.60	14.70	11.70	16.30
MnO	0.21	0.21	0.20	0.22	0.26	0.28	0.21	0.26	0.19	0.23
MgO	7.30	7.51	6.83	9.86	7.33	7.01	11.50	6.32	8.84	7.24
CaO	14.10	12.60	11.20	13.40	9.75	10.00	13.70	10.60	14.10	11.10
Na2O	0.87	1.15	1.63	0.76	2.66	2.20	0.73	2.79	1.02	1.33
K2O	0.13	0.26	0.13	0.09	0.13	0.18	0.17	0.22	0.11	0.14
P2O5	0.10	0.06	0.05	0.03	0.07	0.06	0.03	0.06	0.03	0.04
LOI	0.00	0.00	0.00	0.23	0.70	0.31	0.47	1.23	0.54	0.00
TOTAL	98.20	99.60	99.10	100.50	100.40	99.30	100.30	99.90	100.20	98.90
Trace elements (ppm)										
Sc	49.7	43.8	45.5	42.9	44.2	48.6	56.4	46.4	46.6	47.4
V	37	29	29	15	31	62	18	39	10	15
Cr	540	310	150	220	250	71	570	100	410	200
C0	23	23	25	24	65	38	19	16	11	20
Ni	75	47	35	56	63	24	44	26	30	58
Cu	151.0	123.0	122.0	221.0	110.0	36.5	89.0	42.4	110.0	249.0
Zn	17.0	12.8	15.1	10.3	23.0	30.4	10.5	16.7	6.3	22.6
Rb	*	*	*	*	*	*	*	*	*	*
Sr	216	94	82	92	50	54	110	88	91	83
Y	9	9	5	0	11	15	0	13	4	7
Zr	48	25	14	0	17	28	0	19	7	7
Nb	*	*	*	0.0	4.0	0.0	6.0	4.0	2.1	0.0
Sb	4.5	2.9	2.1	2.1	1.7	0.5	1.8	1.2	1.0	2.3
Cs	*	*	*	0	0	1	0	2	1	0
Hf	1.9	*	*	*	*	*	*	*	*	*
Ta		*	*	*	*	*	*	*	*	*
W	62	87	140	60	240	140	50	0	48	52
Pb	nd	nd	nd	nd	nd	nd	nd	nd	nd	nd
Th	nd	nd	nd	nd	nd	nd	nd	nd	nd	nd
U	nd	nd	nd	0	0	0	0	49	nd	0
Ba	23	56	73	32	94	67	39	91	41	55
Rare earth elements (ppm)										
La	4.4	nd	nd	0.2	1.3	nd	nd	nd	nd	nd
Ce	11.0	nd		1.0	4.0	nd	nd	nd	nd	nd
Pr	nd	nd	nd	nd	nd	nd	nd	nd	nd	nd
Nd	8.0	nd	nd	*	3.0	nd	nd	nd	nd	nd
Sm	2.4	nd	nd	0.2	1.1	nd	nd	nd	nd	nd
Eu	1.2	nd	nd	0.3	0.3	nd	nd	nd	nd	nd
Gd	nd	nd	nd	nd	nd	nd	nd	nd	nd	nd
Tb	0.5	nd	nd	0.1	0.4	nd	nd	nd	nd	nd
Dy	nd	nd	nd	nd	nd	nd	nd	nd	nd	nd
Ho	nd	nd	nd	nd	nd	nd	nd	nd	nd	nd
Er	nd	nd	nd	nd	nd	nd	nd	nd	nd	nd
Tm	nd	nd	nd	nd	nd	nd	nd	nd	nd	nd
Yb	1.7	nd	nd	0.5	2.1	nd	nd	nd	nd	nd
Lu	0.3	nd	nd	0.1	0.3	nd	nd	nd	nd	nd

Table 1a. (Continued)

Sample	Ga3625	Ga3628	Kj3721	Kj3722	Mg3633	Mg3634	MgA3636	MgA3637	Mg3638	Mg3639
Major elements (wt%)										
SiO2	48.20	47.80	47.10	48.00	45.50	49.10	52.00	46.50	45.80	47.50
TiO2	0.14	0.40	0.16	0.79	0.54	0.68	0.32	0.32	0.66	0.16
Al2O3	15.20	15.30	15.80	13.30	13.20	14.30	12.90	15.90	12.40	13.50
Fe2O3T	12.20	14.20	11.60	12.60	16.30	16.00	17.10	13.60	20.20	12.70
MnO	0.19	0.22	0.20	0.18	0.21	0.22	0.23	0.24	0.28	0.19
MgO	8.79	6.92	8.99	9.16	9.63	5.27	6.72	7.97	7.06	10.40
CaO	13.00	11.70	13.60	12.20	11.60	11.20	10.30	12.80	11.40	13.50
Na2O	1.42	1.47	0.66	1.61	1.62	1.05	0.61	0.95	0.86	1.08
K2O	0.15	0.16	0.15	0.24	0.16	0.26	0.13	0.22	0.19	0.08
P2O5	0.02	0.06	0.02	0.08	0.06	0.07	0.06	0.06	0.07	0.03
LOI	0.16	0.16	0.77	0.62	0.00	0.47	0.00	0.70	0.00	0.00
TOTAL	99.50	98.40	99.10	98.80	98.40	98.60	99.70	99.30	98.70	99.00
Trace elements (ppm)										
Sc	49.8	40.1	44.3	41.2	45.3	41.9	42.2	52.4	57.7	55.4
V	19	38	19	25	26	66	32	45	86	19
Cr	190	260	82	310	600	87	270	180	160	470
C0	25	50	26	24	18	30	25	58	43	20
Ni	35	60	35	32	62	33	65	31	86	52
Cu	91.6	759.0	188.0	59.4	151.0	105.0	166.0	51.7	275.0	192.0
Zn	11.4	28.8	10.3	10.2	12.9	23.6	19.4	28.4	47.1	8.9
Rb	*	*	*	*	*	*	*	*	*	*
Sr	103	142		152	81	187	123	194	59	67
Y	*	*	*	5	10	8		4	6	*
Zr	5	20	8	49	19	25	17	7	5	*
Nb	*	*	*	*	*	*	*	*	*	*
Sb	3.6	2.4	0.8	1.1	3.2	2.5	4.0	1.4	2.6	3.7
Cs			1	1		1	1	*	1	1
Hf	*	*	0.5	1.6	*	*	*	*	*	*
Ta	*	*	*	*	*	*	*			
W	160	290	88	68	64	93	100	260	75	93
Pb	nd	nd	nd	nd	nd	nd	nd	nd	nd	nd
Th	nd	nd	nd	nd	nd	nd	nd	nd	nd	nd
U	nd	nd	nd	nd	0	0	nd	nd	nd	nd
Ba	23	128	53	49	41	72	41	68	49	39
Rare earth elements (ppm)										
La	nd	nd	nd	nd	1.7	3.4	nd	1.8	0.9	nd
Ce	nd	nd	nd	nd	4.0	8.0	nd	5.0	3.0	nd
Pr	nd	nd	nd	nd	nd	nd	nd	nd	nd	nd
Nd	nd	nd	nd	nd	3.0	5.0	nd	3.0	3.0	nd
Sm	nd	nd	nd	nd	1.1	1.4	nd	1.2	1.0	nd
Eu	nd	nd	nd	nd	0.8	0.7	nd	0.6	0.4	nd
Gd	nd	nd	nd	nd	nd	nd	nd	nd	nd	nd
Tb	nd	nd	nd	nd	0.4	0.4	nd	0.3	nd	nd
Dy	nd	nd	nd	nd	nd	nd	nd	nd	nd	nd
Ho	nd	nd	nd	nd	nd	nd	nd	nd	nd	nd
Er	nd	nd	nd	nd	nd	nd	nd	nd	nd	nd
Tm	nd	nd	nd	nd	nd	nd	nd	nd	nd	nd
Yb	nd	nd	nd	nd	1.8	1.6	nd	1.3	2.3	nd
Lu	nd	nd	nd	nd	0.3	0.2	nd	0.2	0.4	nd

Table 1a. (Continued)

Sample	Mg3640	Mk3641	Mk3670	Mk3614	Mk3615	Mk3616	Mk3617	Mk3671	Rj3723	Rj3724	Dg6018C
Major elements (wt%)											
SiO2	47.60	47.10	41.80	48.20	49.60	46.50	48.10	44.10	50.60	49.90	55.07
TiO2	0.30	0.30	1.55	0.54	0.11	0.44	0.35	0.75	0.19	0.16	0.26
Al2O3	14.00	14.70	18.90	15.00	12.40	17.40	14.50	15.90	17.10	15.80	13.89
Fe2O3T	15.40	16.70	18.90	13.00	9.77	14.70	14.20	15.90	9.69	7.91	12.50
MnO	0.21	0.20	0.32	0.20	0.19	0.23	0.23	0.23	0.16	0.14	0.21
MgO	8.29	7.39	4.73	6.87	11.80	6.35	8.59	7.76	7.41	9.35	6.38
CaO	12.70	12.40	11.30	11.60	13.90	12.10	13.00	13.00	12.40	13.90	10.41
Na2O	0.91	1.32	1.10	2.06	0.68	0.97	0.75	1.28	1.43	0.89	0.85
K2O	0.14	0.12	0.20	0.15	0.13	0.21	0.20	0.28	0.10	0.10	0.28
P2O5	0.05	0.07	0.56	0.08	0.02	0.06	0.04	0.14	0.03	0.03	0.01
LOI	0.00		0.39	1.16	1.00	0.70	0.31	1.00	0.70	0.77	0.70
TOTAL	99.10	99.10	99.80	98.90	99.60	99.60	100.30	100.40	99.80	99.00	100.56
Trace elements (ppm)											
Sc	46.1	45.5	19.5	41.0	54.8	49.0	52.2	44.9	41.5	34.7	
V	24	26	51	65	10	52	32	82	15	13	371
Cr	460	390	61	100	99	40	120	65	21	210	110
C0	24	45	21	46	16	26	28	33	18	26	37
Ni	53	67	30	27	23	17	27	26	13	20	31
Cu	158.0	357.0	94.3	277.0	240.0	34.8	75.0	93.9	63.6	28.5	41.0
Zn	12.1	12.9	37.4	25.0	7.9	22.3	13.5	33.7	6.2	6.8	108.0
Rb	*	*	*	0.2	*	*	*	*	*	*	14.0
Sr	67	110	529	194	66	154	108	320	98	103	95
Y	4	5	2	10	0	0	7	6	*	*	*
Zr	11	15	13	30	0	12	0	28	12	11	12
Nb	*	*	*	0.0	0.0	4.0	0.0	3.0	*	*	4.0
Sb	3.5	4.7	1.3	1.3	0.9	0.7	1.5	1.1	0.5	0.7	*
Cs	*	*	*	*	1	1	1	*	*	1	*
Hf	*	*	*	*	*	*	*	1.0	*	*	*
Ta		1	*	*	*	*	*	*	*	*	*
W	130	210	57	170	83	100	120	100		160	nd
Pb	nd	nd	nd	nd	nd	nd	nd	3	nd	nd	nd
Th	nd	nd	nd	nd	nd	nd	nd	nd	nd	nd	nd
U	nd	nd	nd	0	nd	nd	nd	nd	nd	nd	nd
Ba	49	17	53	52	42	53	69	66	48	31	79
Rare earth elements (ppm)											
La	nd	nd	nd	3.1	nd	2.0	nd	nd	1.2	nd	nd
Ce	nd	nd	nd	8.0	nd	4.0	nd	nd	3.0	nd	nd
Pr	nd	nd	nd	nd	nd	nd	nd	nd	nd	nd	nd
Nd	nd	nd	nd	6.0	nd	nd	nd	nd	nd	nd	nd
Sm	nd	nd	nd	1.8	nd	0.6	nd	nd	0.4	nd	nd
Eu	nd	nd	nd	0.9	nd	0.3	nd	nd	0.5	nd	nd
Gd	nd	nd	nd	nd	nd	nd	nd	nd	nd	nd	nd
Tb	nd	nd	nd	0.5	nd	0.1	nd	nd	0.1	nd	nd
Dy	nd	nd	nd	nd	nd	nd	nd	nd	nd	nd	nd
Ho	nd	nd	nd	nd	nd	nd	nd	nd	nd	nd	nd
Er	nd	nd	nd	nd	nd	nd	nd	nd	nd	nd	nd
Tm	nd	nd	nd	nd	nd	nd	nd	nd	nd	nd	nd
Yb	nd	nd	nd	2.1	nd	0.5	nd	nd	0.8	nd	nd
Lu	nd	nd	nd	0.3	nd	0.1	nd	nd	0.1	nd	nd

Table 1b. Geleba mafic rocks, southern part of the Megado Belt

Sample	G97027b	G97027c	G97029	G97031	G97035	G97037A	97037Aa	G97037B	G97037C	G97037D
Major elements (wt%)										
SiO2	55.30	55.75	52.60	48.13	56.71	49.98	51.71	56.06	49.97	51.19
TiO2	1.08	1.31	2.01	0.41	0.26	0.69	0.67	0.41	0.71	0.51
Al2O3	14.59	12.35	14.18	15.40	15.65	15.62	15.00	2.82	14.06	5.33
Fe2O3T	8.87	7.97	6.17	9.81	8.20	8.10	7.14	6.98	7.71	10.80
MnO	0.18	0.17	0.31	0.16	0.15	0.13	0.14	0.12	0.14	0.19
MgO	5.06	1.03	3.69	7.81	2.60	8.78	9.85	27.06	10.73	24.66
CaO	8.54	14.24	14.28	12.10	9.39	10.89	12.94	0.37	12.29	3.11
Na2O	4.24	1.27	4.45	2.57	1.30	2.64	2.54	0.24	1.83	0.31
K2O	0.86	0.08	0.32	0.37	0.43	0.25	0.06	0.03	0.22	0.01
P2O5	0.21	0.25	0.70	0.02	0.04	0.04	0.03	0.12	0.03	0.04
LOI	1.50	4.36	0.47	3.41	4.70	3.75	0.69	6.58	1.47	4.63
TOTAL	100.45	98.80	99.19	100.19	99.45	100.88	100.78	100.79	99.17	100.77
Trace elements (ppm)										
Cr	126	*	25	563	285	405	366	1617	458	2866
Co	43	60	21	53	52	52	53	61	48	66
Ni	53	10	*	164	50	83	80	1437	145	441
Cu	*	*	*	13	*	19	35	*	3	35
Zn	37	*	46	57	19	36	24	124	54	83
Rb	17	14	14	18	15	12	12	7	14	11
Sr	334	790	452	119	137	399	342	37	297	44
Y	41	109	39	11	*	10	9	4	10	4
Zr	209	831	122	17	43	35	30	29	41	25
Nb	12	33	9	5	7	6	5	7	6	6
Ba	231	92	209	98	92	52	53	19	85	23
Rare earth elements (ppm)										
La	24.0	nd	nd	15.9	nd	nd	nd	9.6	nd	nd
Ce	42.5	nd	nd	6.8	nd	nd	nd	12.7	nd	nd
Pr	5.3	nd	nd	0.4	nd	nd	nd	1.0	nd	nd
Nd	23.2	nd	nd	2.0	nd	nd	nd	4.7	nd	nd
Sm	5.9	nd	nd	0.8	nd	nd	nd	1.1	nd	nd
Eu	1.6	nd	nd	0.4	nd	nd	nd	0.1	nd	nd
Gd	6.3	nd	nd	1.3	nd	nd	nd	1.0	nd	nd
Tb	1.0	nd	nd	0.3	nd	nd	nd	0.1	nd	nd
Dy	6.7	nd	nd	1.8	nd	nd	nd	1.0	nd	nd
Ho	1.3	nd	nd	0.4	nd	nd	nd	0.2	nd	nd
Er	4.1	nd	nd	1.3	nd	nd	nd	0.6	nd	nd
Tm	0.6	nd	nd	0.2	nd	nd	nd	0.1	nd	nd
Yb	8.2	nd	nd	1.5	nd	nd	nd	7.8	nd	nd

Table 1b. (Continued)

Sample	G97042	G97043	G97045A	G97045B	G97033	G97041	G97047	G97048	G97050	G97055
Major elements (wt%).										
SiO2	53.94	56.84	56.84	55.27	59.16	60.29	63.54	65.18	66.18	59.91
TiO2	1.12	1.21	0.62	0.49	0.23	1.01	0.62	0.45	0.48	0.80
Al2O3	14.68	14.38	15.03	14.14	8.99	14.42	15.71	17.91	17.41	15.69
Fe2O3T	6.45	6.62	6.19	12.38	8.43	5.12	6.87	3.59	4.14	7.53
MnO	0.11	0.11	0.16	0.16	0.17	0.08	0.16	0.06	0.09	0.09
MgO	5.25	4.96	1.89	5.25	9.65	3.55	3.24	1.23	1.39	3.37
CaO	6.08	5.71	12.21	9.71	924.00	4.35	5.88	5.59	4.94	6.64
Na2O	3.48	3.35	3.33	1.55	1.49	3.24	3.29	4.57	4.82	3.12
K2O	1.85	2.05	0.18	0.28	0.23	3.20	1.30	1.03	1.21	1.55
P2O5	0.26	0.28	0.13	0.08	0.07	0.26	0.15	0.14	0.19	0.17
LOI	7.81	4.29	4.14	1.72	2.90	3.86	0.47	0.41	0.52	0.57
TOTAL	**101.02**	**99.80**	**100.72**	**101.05**	**100.56**	**99.39**	**101.23**	**100.15**	**101.36**	**99.46**
Trace elements (ppm)										
Cr	222	216	9	31	29	166	61	16	*	38
Co	36	41	39	52	50	30	45	35	45	50
Ni	109	96	11	14	*	70	16	*	*	14
Cu	26	25	*	77	53	4	135	14	73	77
Zn	53	47	*	29	62	28	56	*	22	30
Rb	39	60	13	15	16	77	30	39	19	44
Sr	665	639	431	198	167	523	482	676	571	449
Y	15	18	102	5	*	16	19	3	5	13
Zr	152	166	453	22	15	195	34	59	56	63
Nb	11	13	18	4	6	14	9	6	6	7
Ba	696	677	93	105	197	887	659	618	626	512
Rare earth elements (ppm)										
La	nd	32.6	59.5	10.0	nd	nd	nd	nd	nd	nd
Ce	nd	58.0	138.1	5.9	nd	nd	nd	nd	nd	nd
Pr	nd	6.7	17.6	0.4	nd	nd	nd	nd	nd	nd
Nd	nd	26.6	78.5	2.0	nd	nd	nd	nd	nd	nd
Sm	nd	5.3	20.1	0.6	nd	nd	nd	nd	nd	nd
Eu	nd	1.5	5.5	0.2	nd	nd	nd	nd	nd	nd
Gd	nd	4.7	20.2	0.8	nd	nd	nd	nd	nd	nd
Tb	nd	0.6	3.2	0.1	nd	nd	nd	nd	nd	nd
Dy	nd	3.4	18.2	1.1	nd	nd	nd	nd	nd	nd
Ho	nd	0.6	3.3	0.2	nd	nd	nd	nd	nd	nd
Er	nd	1.7	9.7	0.7	nd	nd	nd	nd	nd	nd
Tm	nd	0.2	1.4	0.1	nd	nd	nd	nd	nd	nd
Yb	nd	5.9	9.2	0.8	nd	nd	nd	nd	nd	nd

Table 1c. Mafic rocks of the Moyale-El Kur and Bulbul belts

Sample	Bl96079	Bl96080	Bl96083	Bl96085	Bl96086C	Gn96074	Gn98025	JE97126	JE97127	JE97128
Major elements (wt%).										
SiO2	47.75	49.88	53.41	52.64	56.84	48.43	46.87	29.74	50.30	45.77
TiO2	3.03	1.05	0.98	0.83	0.52	2.04	1.66	0.12	0.88	0.22
Al2O3	12.96	14.58	21.21	20.90	20.06	16.10	14.96	1.07	13.08	2.41
Fe2O3	1.61	1.15	0.63	0.81	0.63	1.31	1.23	0.60	0.88	0.53
FeO	14.46	10.31	5.69	7.26	5.64	11.73	11.04	5.37	7.90	4.78
Fe2O3T	16.07	11.46	6.32	8.07	6.27	13.04	12.27	5.97	8.78	5.31
MnO	0.24	0.37	0.05	0.16	0.12	0.19	0.19	0.09	0.16	0.09
MgO	5.14	5.11	4.59	2.49	1.00	4.15	6.31	37.27	9.65	25.69
CaO	8.90	15.61	5.80	8.42	8.36	8.90	11.26	0.79	15.29	11.54
Na2O	3.07	0.49	6.38	4.12	6.36	5.76	3.73	0.00	1.50	0.00
K2O	0.87	0.03	0.10	1.07	0.25	0.63	0.55	0.02	0.08	0.00
P2O5	0.55	0.18	0.26	0.26	0.26	0.68	0.29	0.04	0.06	0.01
LOI	0.29	0.33	1.41	0.41	0.31	0.55	1.62	24.82	2.08	7.73
TOTAL	**98.88**	**99.09**	**100.52**	**99.37**	**100.35**	**100.47**	**99.70**	**99.95**	**101.86**	**98.79**
Trace elements (ppm)										
V	425	273	127	141	106	205	318	*	293	202
Cr	59	31	53		12	126	180	935	380	5539
Co	38	23	15	15	*	35	34	58	51	42
Ni	35	30	19	*	*	73	87	1657	92	566
Cu	62	*	*	27	*	8	*	*	68	39
Zn	141	71	35	79	31	83	82	20	35	18
Rb	28	14	5	31	7	16	4	3	15	8
Sr	321	529	458	802	1235	1208	516	45	127	37
Y	48	36	16	19	11	29	24	*	12	*
Zr	233	87	139	79	89	130	74	9	47	8
Nb	13	8	8	6	10	8	7	5	6	5
Sb	nd	nd	nd	nd	nd	nd	nd	nd	nd	nd
Cs	nd	nd	nd	nd	nd	nd	nd	nd	nd	nd
Hf	nd	3	nd	nd	nd	nd	nd	nd	nd	nd
Ta	nd	0	nd	nd	nd	nd	nd	nd	nd	nd
W	nd	nd	nd	nd	nd	nd	nd	nd	nd	nd
Pb	nd	nd	nd	nd	nd	nd	nd	nd	nd	nd
Th	nd	1	nd	nd	nd	nd	nd	nd	nd	nd
U	nd	1	nd	nd	nd	nd	nd	nd	nd	nd
Ba	524	24	39	611	128	611	121	13	29	24
Rare earth elements (ppm)										
La	nd	17.5	nd	nd	nd	nd	16.9	nd	nd	nd
Ce	nd	38.6	nd	nd	nd	nd	50.9	nd	nd	nd
Pr	nd	nd	nd	nd	nd	nd	3.6	nd	nd	nd
Nd	nd	22.4	nd	nd	nd	nd	17.0	nd	nd	nd
Sm	nd	5.5	nd	nd	nd	nd	5.0	nd	nd	nd
Eu	nd	2.0	nd	nd	nd	nd	2.1	nd	nd	nd
Gd	nd	5.5	nd	nd	nd	nd	5.0	nd	nd	nd
Tb	nd	1.0	nd	nd	nd	nd	1.1	nd	nd	nd
Dy	nd	nd	nd	nd	nd	nd	5.0	nd	nd	nd
Ho	nd	nd	nd	nd	nd	nd	1.2	nd	nd	nd
Er	nd	nd	nd	nd	nd	nd	2.8	nd	nd	nd
Tm	nd	0.5	nd	nd	nd	nd	0.7	nd	nd	nd
Yb	nd	3.7	nd	nd	nd	nd	5.5	nd	nd	nd
Lu	nd	0.5	nd	nd	nd	nd	nd	nd	nd	nd

Bl = Bulbul mafic rocks.

JE = Jimma El Kur mafic rocks.

M1 = Western Moyale mafic rocks.

M2 = Eastern Moyale mafic rocks.

Gn = Gneissose amphibolite intercalated with high-grade quartzofeldspathic gneisses.

Table 1c. (Continued)

Sample	JE97132c	JE97132d	JE97144	JE97145	M19608	M197077	M197080	M197081A	M197081B	M197082
Major elements (wt%).										
SiO2	56.43	52.52	55.17	56.28	46.25	55.07	54.66	55.17	55.98	51.39
TiO2	2.30	0.64	0.84	0.96	0.12	0.68	0.29	0.30	0.35	0.60
Al2O3	14.62	13.39	15.08	16.07	26.96	14.13	1.95	1.91	4.50	10.26
Fe2O3	1.00	0.73	0.79	0.73	0.24	0.60	0.92	1.14	1.04	0.82
FeO	9.00	6.54	7.10	6.53	2.12	5.35	8.27	10.22	9.37	7.34
Fe2O3T	10.00	7.27	7.89	7.26	2.36	5.95	9.19	11.36	10.41	8.16
MnO	0.17	0.12	0.08	0.11	0.06	0.11	0.18	0.23	0.20	0.15
MgO	3.46	10.38	2.25	3.13	4.74	8.08	19.54	19.29	15.39	14.15
CaO	5.49	13.14	5.26	7.17	15.11	12.85	12.70	7.88	11.15	12.98
Na2O	3.84	0.90	4.06	4.60	2.11	1.96	0.63	0.18	0.29	0.65
K2O	2.80	0.41	3.38	2.04	0.28	0.10	0.05	0.05	0.38	0.23
P2O5	0.83	0.06	0.27	0.33	0.00	0.02	0.01	0.04	0.05	0.04
LOI	0.65	1.41	6.11	2.51	2.05	2.24	1.65	3.82	2.08	1.31
TOTAL	**100.60**	**100.25**	**100.39**	**100.45**	**100.05**	**101.21**	**100.84**	**100.25**	**100.80**	**99.93**
Trace elements (ppm)										
V	178	216	110	149	41	240	198	245	504	282
Cr	16	1014	27	33	588	310	861	1071	1232	2040
Co	32	50	43	32	17	42	59	83	62	52
Ni	24	212	11	20	104	56	81	165	80	338
Cu	18	112	18	19	23	29	29	*	166	*
Zn	116	39	27	47	19	23	40	51	67	56
Rb	76	12	80	41	9	12	13	17	14	19
Sr	638	129	854	870	327	376	50	48	79	68
Y	48	9	16	14	*	8	*	4	7	9
Zr	416	27	192	165	6	27	10	11	24	24
Nb	34	6	13	12	4	5	5	5	7	6
Sb	nd	nd	nd	nd	nd	nd	nd	nd	nd	nd
Cs	nd	nd	nd	nd	nd	nd	nd	nd	nd	nd
Hf	nd	nd	nd	nd	0	nd	nd	nd	nd	nd
Ta	nd	nd	nd	nd	0	nd	nd	nd	nd	nd
W	nd	nd	nd	nd	nd	nd	nd	nd	nd	nd
Pb	nd	nd	nd	nd	nd	nd	nd	nd	nd	nd
Th	nd	nd	nd	nd	0	nd	nd	nd	nd	nd
U	nd	nd	nd	nd	0	nd	nd	nd	nd	nd
Ba	1046	124	1344	447	49	53	46	263	59	118
Rare earth elements (ppm)										
La	72.6	6.4	nd	nd	0.5	4.5	nd	nd	nd	4.9
Ce	142.6	5.3	nd	nd	1.1	5.1	nd	nd	nd	6.9
Pr	17.4	0.6	nd	nd	nd	0.8	nd	nd	nd	0.5
Nd	69.5	3.3	nd	nd	0.5	4.4	nd	nd	nd	2.5
Sm	13.7	1.1	nd	nd	0.2	1.4	nd	nd	nd	0.9
Eu	3.2	0.4	nd	nd	0.3	0.7	nd	nd	nd	0.4
Gd	12.9	1.4	nd	nd	0.3	1.6	nd	nd	nd	1.5
Tb	1.8	0.2	nd	nd	0.1	0.3	nd	nd	nd	0.3
Dy	9.6	1.7	nd	nd	nd	2.0	nd	nd	nd	2.0
Ho	1.8	0.3	nd	nd	nd	0.4	nd	nd	nd	0.4
Er	4.8	1.0	nd	nd	nd	1.1	nd	nd	nd	1.3
Tm	0.7	0.1	nd	nd	nd	0.1	nd	nd	nd	0.2
Yb	4.2	0.9	nd	nd	0.1	4.7	nd	nd	nd	1.2
Lu	nd	nd	nd	nd	0.0	nd	nd	nd	nd	nd

Table 1c. (Continued)

Sample	M197083	M197084	M197084B	M197085	M197086	M197087A	M197088A	M197089	M197090	M197093
Major elements (wt%).										
SiO2	50.91	53.98	56.90	51.04	53.69	52.99	53.05	54.36	47.97	46.83
TiO2	1.23	0.33	0.34	0.65	0.51	0.56	0.51	0.51	2.36	2.28
Al2O3	13.69	3.21	5.56	13.04	14.42	13.63	13.08	13.13	19.62	15.98
Fe2O3	1.36	0.69	0.72	0.82	0.89	0.90	0.72	0.82	1.16	1.37
FeO	12.25	6.23	6.47	7.40	8.04	8.06	6.50	7.41	10.42	12.35
Fe2O3T	13.61	6.92	7.19	8.22	8.93	8.96	7.22	8.23	11.58	13.72
MnO	0.19	0.15	0.17	0.15	0.17	0.14	0.15	0.17	0.14	0.16
MgO	4.84	18.15	16.89	6.63	7.63	8.44	8.79	8.47	5.39	8.71
CaO	4.86	12.98	12.14	8.65	11.05	9.57	12.39	11.42	9.98	10.11
Na2O	2.13	0.49	0.33	1.38	1.59	2.46	3.45	2.79	2.68	1.69
K2O	0.08	0.13	0.23	0.75	0.25	0.66	0.39	0.58	0.14	0.10
P2O5	0.11	0.05	0.03	0.06	0.03	0.05	0.06	0.06	0.03	0.02
LOI	7.02	2.41	1.16	10.31	1.76	1.53	1.79	1.61	0.03	0.41
TOTAL	**98.66**	**98.81**	**100.95**	**100.89**	**100.03**	**98.99**	**100.89**	**101.34**	**99.92**	**100.03**
Trace elements (ppm)										
V	502	148	101	305	261	250	167	263	394	314
Cr	30	3028	2102	289	387	308	327	777	38	123
Co	37	64	64	36	41	44	40	34	49	64
Ni	13	455	492	75	86	100	75	19	28	64
Cu	39	34	*	56	*	19	22	*	*	24
Zn	98	41	55	123	76	66	22	65	70	83
Rb	13	10	12	31	15	25	13	14	14	14
Sr	118	76	52	192	132	117	219	208	570	440
Y	23	4	3	16	10	13	10	26	4	6
Zr	67	19	23	36	29	35	80	68	23	24
Nb	6	7	6	9	5	6	6	8	6	6
Sb	nd	nd	nd	nd	nd	nd	nd	nd	nd	nd
Cs	nd	nd	nd	nd	nd	nd	nd	nd	nd	nd
Hf	nd	nd	nd	nd	nd	nd	nd	nd	nd	nd
Ta	nd	nd	nd	nd	nd	nd	nd	nd	nd	nd
W	nd	nd	nd	nd	nd	nd	nd	nd	nd	nd
Pb	nd	nd	nd	nd	nd	nd	nd	nd	nd	nd
Th	nd	nd	nd	nd	nd	nd	nd	nd	nd	nd
U	nd	nd	nd	nd	nd	nd	nd	nd	nd	nd
Ba	45	29	32	174	71	163	81	140	104	198
Rare earth elements (ppm)										
La	11.1	nd	nd	nd	4.2	nd	9.2	15.3	3.1	nd
Ce	12.2	nd	nd	nd	17.8	nd	10.7	23.3	5.0	nd
Pr	1.4	nd	nd	nd	0.5	nd	1.3	3.4	0.6	nd
Nd	7.8	nd	nd	nd	2.8	nd	6.4	16.2	2.9	nd
Sm	2.5	nd	nd	nd	1.0	nd	1.8	4.2	0.9	nd
Eu	0.9	nd	nd	nd	0.4	nd	0.7	0.9	0.9	nd
Gd	3.2	nd	nd	nd	1.3	nd	2.1	4.6	1.1	nd
Tb	0.6	nd	nd	nd	0.2	nd	0.4	0.8	0.2	nd
Dy	4.3	nd	nd	nd	1.8	nd	2.5	4.9	1.0	nd
Ho	0.9	nd	nd	nd	0.4	nd	0.5	1.0	0.2	nd
Er	2.8	nd	nd	nd	1.3	nd	1.6	3.1	0.6	nd
Tm	0.4	nd	nd	nd	0.2	nd	0.2	0.4	0.1	nd
Yb	2.9	nd	nd	nd	1.4	nd	1.5	6.1	0.5	nd
Lu	nd	nd	nd	nd	nd	nd	nd	nd	nd	nd

Table 1c. (Continued)

Sample	M197094	M197095a	M197095b	M197095c	M197096a	M197096b	M198027	M198032a	M198035	M198036
Major elements (wt%).										
SiO2	47.04	47.90	48.25	49.84	48.24	47.60	48.89	47.82	49.77	50.26
TiO2	2.50	0.88	0.57	0.33	0.71	1.32	1.44	2.58	0.33	0.50
Al2O3	18.85	16.42	19.42	25.25	16.62	16.83	14.17	13.66	13.97	21.06
Fe2O3	1.17	0.69	0.80	0.20	0.66	0.80	1.26	1.49	1.06	0.68
FeO	10.51	6.23	7.22	1.78	5.96	7.22	11.28	13.42	9.47	6.10
Fe2O3T	11.68	6.92	8.02	1.98	6.62	8.02	12.54	14.91	10.53	6.78
MnO	0.17	0.13	0.12	0.05	0.13	0.11	0.18	0.22	0.17	0.14
MgO	7.77	7.45	8.60	1.14	8.99	7.42	7.22	6.14	9.95	5.09
CaO	9.23	15.02	12.20	13.47	13.87	14.83	11.46	9.82	12.42	11.53
Na2O	2.88	1.99	2.97	6.01	2.00	1.78	2.57	2.40	0.73	2.84
K2O	0.12	0.01	0.07	0.18	0.07	0.06	0.40	0.97	0.16	0.04
P2O5	0.03	0.02	0.01	0.02	0.02	0.02	0.16	0.27	0.05	0.03
LOI	-1.21	3.46	0.42	2.22	2.81	3.07	0.79	0.72	0.93	0.69
TOTAL	**99.05**	**100.20**	**100.65**	**100.50**	**100.07**	**101.06**	**99.82**	**99.53**	**99.02**	**98.95**
Trace elements (ppm)										
V	122	295	137	*	211	358	372	463	300	*
Cr	96	311	200	*	379	573	132	196	523	*
Co	49	36	51	18	39	47	32	29	42	*
Ni	58	35	51	*	49	41	57	45	89	*
Cu	*	67	20	*	84	*	91	7	57	*
Zn	49	23	29	*	28	35	97	132	71	65
Rb	13	13	12	8	12	12	5	11		90
Sr	596	413	43	760	429	392	149	201	193	68
Y	*	11	4	*	8	9	34	48	7	24
Zr	22	34	16	14	28	30	95	124	18	8
Nb	7	6	5	6	6	7	6	9	6	11
Sb	nd	nd	nd	nd	nd	nd	nd	nd	nd	nd
Cs	nd	nd	nd	nd	nd	nd	nd	nd	nd	nd
Hf	nd	nd	nd	nd	nd	nd	nd	nd	nd	nd
Ta	nd	nd	nd	nd	nd	nd	nd	nd	nd	nd
W	nd	nd	nd	nd	nd	nd	nd	nd	nd	nd
Pb	nd	nd	nd	nd	nd	nd	nd	nd	nd	nd
Th	nd	nd	nd	nd	nd	nd	nd	nd	nd	nd
U	nd	nd	nd	nd	nd	nd	nd	nd	nd	nd
Ba	61	43	132	132	748	27	106	285	45	182
Rare earth elements (ppm)										
La	nd	nd	nd	19.5	nd	nd	nd	nd	6.8	nd
Ce	nd	nd	nd	3.7	nd	nd	nd	nd	7.8	nd
Pr	nd	nd	nd	0.4	nd	nd	nd	nd	0.9	nd
Nd	nd	nd	nd	1.8	nd	nd	nd	nd	4.1	nd
Sm	nd	nd	nd	0.4	nd	nd	nd	nd	1.1	nd
Eu	nd	nd	nd	0.6	nd	nd	nd	nd	0.4	nd
Gd	nd	nd	nd	0.4	nd	nd	nd	nd	1.3	nd
Tb	nd	nd	nd	0.0	nd	nd	nd	nd	0.2	nd
Dy	nd	nd	nd	0.2	nd	nd	nd	nd	1.4	nd
Ho	nd	nd	nd	0.0	nd	nd	nd	nd	0.3	nd
Er	nd	nd	nd	0.1	nd	nd	nd	nd	0.8	nd
Tm	nd	nd	nd	0.0	nd	nd	nd	nd	0.1	nd
Yb	nd	nd	nd	1.8	nd	nd	nd	nd	0.8	nd
Lu	nd	nd	nd	nd	nd	nd	nd	nd	nd	nd

Table 1c. (Continued)

Sample	M198046a	M198046b	M198051	M297099	M297100	M297101a	M297109a	M297110	M297113b
Major elements (wt%).									
SiO2	54.56	50.26	48.47	51.26	54.52	46.04	47.98	49.70	45.22
TiO2	0.32	0.24	1.35	1.39	0.79	0.44	1.31	1.34	0.21
Al2O3	11.32	5.94	15.13	15.28	14.77	16.16	13.74	13.16	23.11
Fe2O3	0.94	0.88	1.30	1.56	1.22	1.12	1.16	1.22	3.57
FeO	8.47	7.93	11.71	13.97	10.95	10.09	10.45	10.93	3.97
Fe2O3T	9.41	8.81	13.01	15.53	12.17	11.21	11.61	12.15	3.97
MnO	0.20	0.17	0.18	0.22	0.14	0.18	0.20	0.20	0.09
MgO	11.03	20.36	6.83	5.08	3.97	9.74	7.12	6.91	8.90
CaO	10.72	10.74	10.81	9.84	8.38	12.90	9.23	10.45	15.17
Na2O	1.13	0.09	2.23	2.61	3.12	0.67	2.69	2.82	1.24
K2O	0.15	0.00	0.37	0.15	0.12	0.00	0.36	0.21	0.04
P2O5	0.04	0.05	0.18	0.10	0.06	0.00	0.13	0.17	0.00
LOI	1.52	3.02	1.51	-0.48	1.08	2.03	5.01	2.96	2.91
TOTAL	**100.41**	**99.68**	**100.07**	**100.97**	**99.12**	**99.39**	**99.38**	**100.07**	**100.84**
Trace elements (ppm)									
V	141	32	409	485	354	407	297	280	69
Cr	7862	*	253	*	10	160	148	132	746
Co	64	9	37	52	43	51	44	41	37
Ni	546	*	59	10	9	52	56	40	217
Cu	*	*	72	32	183	67	54	96	40
Zn	151	76	102	86	84	53	90	92	21
Rb	*	81	*	19	16	15	24	17	12
Sr	*	288	281	121	150	332	169	165	110
Y	4	31	31	28	20	*	30	33	*
Zr	20	176	90	70	52	10	90	105	10
Nb	6	11	6	5	5	6	11	13	5
Sb	nd	nd	nd	nd	nd	nd	nd	nd	nd
Cs	nd	nd	nd	nd	nd	nd	nd	nd	nd
Hf	nd	nd	nd	nd	nd	nd	nd	nd	nd
Ta	nd	nd	nd	nd	nd	nd	nd	nd	nd
W	nd	nd	nd	nd	nd	nd	nd	nd	nd
Pb	nd	nd	nd	nd	nd	nd	nd	nd	nd
Th	nd	nd	nd	nd	nd	nd	nd	nd	nd
U	nd	nd	nd	nd	nd	nd	nd	nd	nd
Ba	6	1230	117	72	49	27	104	nd	35
Rare earth elements (ppm)									
La	14.7	25.5	12.7	10.0	7.0	1.2	13.8	nd	nd
Ce	7.9	3.4	20.1	8.6	9.3	2.8	15.8	nd	nd
Pr	1.1	0.3	2.6	1.3	1.2	0.2	2.1	nd	nd
Nd	5.1	1.7	13.2	7.4	6.2	1.1	10.3	nd	nd
Sm	1.6	0.5	3.8	2.7	2.1	0.5	3.3	nd	nd
Eu	0.5	0.2	1.4	1.1	0.8	0.2	1.3	nd	nd
Gd	1.8	0.6	4.6	3.4	2.9	0.5	4.4	nd	nd
Tb	0.3	0.1	0.8	0.7	0.6	0.1	0.8	nd	nd
Dy	2.1	0.7	5.9	5.1	3.9	0.6	5.4	nd	nd
Ho	0.5	0.1	1.2	1.1	0.8	0.1	1.1	nd	nd
Er	1.3	0.4	3.3	3.3	2.5	0.4	3.3	nd	nd
Tm	0.2	0.1	0.5	0.5	0.4	0.1	0.5	nd	nd
Yb	1.3	0.5	3.3	7.5	2.4	0.5	3.2	nd	nd
Lu	nd	nd	nd	nd	nd	nd	nd	nd	nd